

Neuronal Excitability

Unraveling Synaptic GCaMP Signals: Differential Excitability and Clearance Mechanisms Underlying Distinct Ca^{2+} Dynamics in Tonic and Phasic Excitatory, and Aminergic Modulatory Motor Terminals in *Drosophila*

Xiaomin Xing, and  Chun-Fang Wu<http://dx.doi.org/10.1523/ENEURO.0362-17.2018>

Department of Biology, University of Iowa, Iowa City, IA 52242

Abstract

GCaMP is an optogenetic Ca^{2+} sensor widely used for monitoring neuronal activities but the precise physiological implications of GCaMP signals remain to be further delineated among functionally distinct synapses. The *Drosophila* neuromuscular junction (NMJ), a powerful genetic system for studying synaptic function and plasticity, consists of tonic and phasic glutamatergic and modulatory aminergic motor terminals of distinct properties. We report a first simultaneous imaging and electric recording study to directly contrast the frequency characteristics of GCaMP signals of the three synapses for physiological implications. Different GCaMP variants were applied in genetic and pharmacological perturbation experiments to examine the Ca^{2+} influx and clearance processes underlying the GCaMP signal. Distinct mutational and drug effects on GCaMP signals indicate differential roles of Na^+ and K^+ channels, encoded by genes including *paralytic (para)*, *Shaker (Sh)*, *Shab*, and *ether-a-go-go (eag)*, in excitability control of different motor terminals. Moreover, the Ca^{2+} handling properties reflected by the characteristic frequency dependence of the synaptic GCaMP signals were determined to a large extent by differential capacity of mitochondria-powered Ca^{2+} clearance mechanisms. Simultaneous focal recordings of synaptic activities further revealed that GCaMPs were ineffective in tracking the rapid dynamics of Ca^{2+} influx that triggers transmitter release, especially during low-frequency activities, but more adequately reflected cytosolic residual Ca^{2+} accumulation, a major factor governing activity-dependent synaptic plasticity. These results highlight the vast range of GCaMP response patterns in functionally distinct synaptic types and provide relevant information for establishing basic guidelines for the physiological interpretations of presynaptic GCaMP signals from in situ imaging studies.

Key words: ion channels; mitochondria; octopamine; PMCA; residual calcium; synaptic plasticity

Significance Statement

GCaMPs are a family of genetically encoded Ca^{2+} indicators widely employed in monitoring neuronal circuit activities. This study employed a genetic model system to enable simultaneous recording of presynaptic GCaMP signals in three functionally distinct types of synapses side by side. The results reveal how differential control by membrane excitability and mitochondria-powered Ca^{2+} clearance mechanisms shape distinct residual Ca^{2+} dynamics in different synaptic boutons during repetitive firing. Our results demonstrate a wide range of GCaMP response patterns in relation to different types of synaptic transmission and thereby provide background information for proper interpretations of GCaMP signals in a variety of synaptic activities.

Introduction

Ca²⁺ influx on action potential arrival at synaptic terminals triggers neurotransmitter release, and residual Ca²⁺ accumulation following repetitive action potentials regulates activity-dependent synaptic plasticity (Katz and Miledi, 1967, 1968; Zucker and Regehr, 2002). Na⁺ and K⁺ channels play fundamental roles in shaping the axonal action potential and its repetitive firing pattern (Hille, 2001) and thus can profoundly influence the amplitudes and kinetics of synaptic Ca²⁺ elevation. Conversely, Ca²⁺ clearance mechanisms, including mitochondrial and endoplasmic reticulum (ER) sequestration (Tang and Zucker, 1997; Suzuki et al., 2002; Klose et al., 2009) and energy-dependent extrusion via plasma membrane Ca²⁺-ATPase (PMCA; Dipolo and Beaugé, 1979; Lnenicka et al., 2006), are critical in the restoration of synaptic basal Ca²⁺ levels.

GCaMPs are widely used genetically encoded Ca²⁺ indicators (Nakai et al., 2001; Chen et al., 2013). Despite the frequent applications of GCaMPs in monitoring neuronal activities in nervous systems of various animal species (Wang et al., 2003; Reiff et al., 2005; Rickgauer et al., 2014), it is unclear how differences in membrane excitability and Ca²⁺ clearance mechanisms determine the amplitude and kinetics of GCaMP Ca²⁺ signals in functionally distinct categories of synapses.

We analyzed GCaMP signals in the *Drosophila* larval neuromuscular junction (NMJ), in which both excitatory (glutamatergic tonic type Ib and phasic type Is) as well as modulatory (octopaminergic type II) synapses could be monitored simultaneously within the same optical microscopy field (Johansen et al., 1989; Keshishian et al., 1993; Kurdyak et al., 1994; Monastirioti et al., 1995; Hoang and Chiba, 2001). The glutamatergic type I synapses have been extensively studied for their electrophysiological properties (Jan and Jan, 1976; Ueda and Wu, 2006, 2012; Berke et al., 2013) and striking phenotypes caused by ion channel mutations (for review, see Ganetzky and Wu, 1986; Fox et al., 2005; Frolov et al., 2012). Octopaminergic type II synaptic terminals are known to modulate the growth and transmission properties of type I synapses (Koon et al., 2011) and to display remarkable excitability-dependent plasticity (Budnik et al., 1990; Zhong et al.,

1992; Zhong and Wu, 2004). However, differences in excitability control and Ca²⁺ handling properties among these three distinct synaptic types remain to be determined.

This decade-long study, extended from earlier results (Ueda and Wu, 2006, 2009a; Xing, 2014), employed different versions of GCaMPs, including GCaMPs 1, 5, and 6, to delineate the distinct frequency characteristics of GCaMP signals from type Ib, Is, and II synapses and their preferential sensitivities to different pharmacological or genetic perturbations. In particular, our results show that type II synapses were most strongly affected by manipulations of channels encoded by *ether-a-go-go* (*eag*, Eag, or K_v10 ortholog; for details, see Materials and Methods), *Shab* (K_v2 ortholog), and *paralytic* (*para*, Na_v1) channels, whereas type Is synapses were most severely modified by manipulations of *Shaker* (*Sh*, K_v1 ortholog). Strikingly, double insults through manipulating *Sh* together with either *eag* or *Shab* could generate extreme hyperexcitability in type Is synapses, leading to greatly enhanced GCaMP signals on individual nerve stimulation. In contrast, type Ib synapses remained largely intact in the above experiments but could display similar extreme hyperexcitability following triple insults with combinations of mutations or blockers of K⁺ channels. Simultaneous focal electrical recordings of synaptic activities revealed that such extreme cases of enhanced GCaMP signals actually resulted from supernumerary high-frequency (>100 Hz) repetitive firing in the motor terminals following each single stimulus.

Further kinetic analysis revealed different Ca²⁺ clearance capacity among three types of synaptic terminals. We found that Na⁺ and K⁺ channel mutations or blockers influence mainly the rise kinetics of GCaMP signals, whereas inhibiting Ca²⁺ clearance mediated by PMCA (via high pH treatment) slowed the decay phase acutely. In addition, we discovered that long-term inhibition of mitochondrial energy metabolism by incubation with either 2,4-dinitrophenol (DNP; cf. Greenawalt et al., 1964) or azide (cf. Bowler et al., 2006) led to drastically lengthened decay time of the GCaMP signal and significantly altered its frequency responses to repetitive stimulation, over a time course of tens of minutes.

Overall, this study demonstrates a wide range of GCaMP response patterns indicating differential membrane excitability and Ca²⁺ clearance mechanisms in functionally distinct types of synapses. Although the slow kinetics of GCaMP signals could not adequately resolve the rapid process of Ca²⁺ influx triggered by individual action potentials, they could nevertheless report cytosolic residual Ca²⁺ accumulation on repetitive synaptic activities. Our data thus provide essential baseline information for refined interpretations of GCaMP signals when monitoring *in vivo* neural circuit activities that often result from interplay among different categories of synapses.

Materials and Methods

Fly stocks

All stocks were maintained at room temperature (22–24°C). The Gal4-UAS system was employed for targeted expression of different *GCaMP* versions in the motor neu-

Received October 13, 2017; accepted February 2, 2018; First published February 8, 2018.

The authors declare no competing financial interests.

Author contributions: X.X. and C.-F.W. designed research; X.X. performed research; X.X. and C.-F.W. analyzed data; X.X. and C.-F.W. wrote the paper.

This work was supported by Department of Health and Human Services National Institutes of Health Grants GM88804, AG047612, and AG051513.

Acknowledgment: We thank Drs. Yalin Wang, Yi Zhong, and Troy Littleton for providing GCaMP fly stocks. We thank Mr. Anthony McGregor, Mr. Timothy Patience and Dr. Yu Li for help in proofreading. We also thank Drs. Atulya Iyengar and Atsushi Ueda for discussion of content.

Correspondence should be addressed to either of the following: Dr. Chunfang Wu, Department of Biology, University of Iowa, Iowa City, IA 52242, E-mail: chun-fang-wu@uiowa.edu; or Xiaomin Xing, Department of Biology, University of Iowa, Iowa City, IA 52242, E-mail: xiaomin-xing@uiowa.edu.
<http://dx.doi.org/10.1523/ENEURO.0362-17.2018>

Copyright © 2018 Xing and Wu

This is an open-access article distributed under the terms of the Creative Commons Attribution 4.0 International license, which permits unrestricted use, distribution and reproduction in any medium provided that the original work is properly attributed.

Table 1. Maximum ΔF/F for type I and II synapses of different genotypes

Genotypes	Type Ib		Type Is		Type II	
	40 Hz max ΔF/F ± SD (n, N)	2 Hz max ΔF/F ± SD (n, N)	10 Hz max ΔF/F ± SD (n, N)	20 Hz max ΔF/F ± SD (n, N)	2 Hz max ΔF/F ± SD (n, N)	10 Hz max ΔF/F ± SD (n, N)
0.1 mM Ca ²⁺						
WT	0.16 ± 0.11 (53, 9)	0.07 ± 0.04 (94, 14)	0.08 ± 0.07 (96, 14)	0.43 ± 0.29 (96, 14)	0.12 ± 0.07 (64, 13)	0.57 ± 0.39 (67, 13)
WT + 4AP	1.00 ± 0.33 (18, 3)***	0.21 ± 0.12 (32, 4)***	0.83 ± 0.33 (32, 4)***	1.14 ± 0.41 (32, 4)***	0.24 ± 0.15 (21, 4)**	1.00 ± 0.40 (21, 4)***
WT + TEA	0.91 ± 0.43 (22, 4)***	0.12 ± 0.07 (32, 5)*	0.12 ± 0.08 (32, 5)*	0.86 ± 0.42 (31, 5)***	0.71 ± 0.48 (18, 5)***	1.02 ± 0.57 (19, 5)***
<i>Sh^M</i>	0.63 ± 0.54 (46, 7)***	0.11 ± 0.05 (82, 9)*	0.67 ± 0.27 (82, 9)***	1.10 ± 0.40 (81, 9)***	0.18 ± 0.07 (44, 6)**	0.67 ± 0.31 (44, 6)
<i>Sh¹²⁰</i>	0.18 ± 0.11 (20, 4)	0.08 ± 0.05 (42, 4)	0.63 ± 0.24 (42, 4)***	0.99 ± 0.22 (42, 4)***	0.18 ± 0.09 (29, 3)*	0.64 ± 0.23 (29, 3)
<i>eag¹</i>	0.23 ± 0.18 (39, 6)*	0.09 ± 0.08 (30, 7)	0.10 ± 0.09 (30, 7)	0.59 ± 0.32 (28, 7)*	0.13 ± 0.13 (18, 5)	0.42 ± 0.37 (20, 5)
<i>eag¹ Sh¹²⁰</i>	0.59 ± 0.41 (28, 6)***	0.43 ± 0.34 (89, 12)***	0.83 ± 0.66 (89, 13)***	0.89 ± 0.76 (94, 13)***	0.17 ± 0.10 (26, 10)*	0.34 ± 0.33 (26, 9)
<i>para^{bss1}</i>	0.22 ± 0.21 (49, 6)	0.07 ± 0.04 (71, 8)	0.35 ± 0.55 (71, 8)**	0.64 ± 0.48 (54, 9)**	0.46 ± 0.26 (56, 10)***	0.61 ± 0.39 (55, 10)
<i>para^{ts1}</i>	0.07 ± 0.08 (20, 6)*	0.08 ± 0.08 (47, 7)	0.08 ± 0.05 (47, 7)	0.32 ± 0.20 (47, 7)*	0.11 ± 0.06 (28, 7)	0.25 ± 0.20 (28, 7)***
<i>para^{bss1} Sh¹²⁰</i>	0.36 ± 0.23 (35, 6)***	0.17 ± 0.13 (35, 6)**	0.68 ± 0.46 (35, 6)***	0.89 ± 0.64 (35, 6)***	0.30 ± 0.24 (22, 5)***	0.61 ± 0.40 (22, 5)
0.5 mM Ca ²⁺						
WT	1.11 ± 0.26 (20, 5)***	0.12 ± 0.12 (35, 5)*	0.43 ± 0.16 (44, 5)***	1.22 ± 0.50 (38, 5)***	0.33 ± 0.17 (29, 4)***	0.85 ± 0.40 (33, 5)**
<i>Sh¹²⁰</i>	0.93 ± 0.26 (25, 4)+	0.11 ± 0.04 (13, 2)	0.85 ± 0.24 (22, 3)+++	1.15 ± 0.19 (22, 3)	0.44 ± 0.23 (31, 4)	1.23 ± 0.52 (31, 4)+++
<i>para^{bss1}</i>	0.68 ± 0.14 (26, 3)+++	0.08 ± 0.04 (47, 4)	0.42 ± 0.28 (49, 4)	1.21 ± 0.55 (48, 4)	0.73 ± 0.36 (17, 4)+++	0.98 ± 0.36 (16, 4)

Data are presented as max ΔF/F ± SD (n, N), where n indicates total bouton number and N, NMJ number. N.D., not determined. Bolded numbers are significantly different from WT control (0.1 mM Ca²⁺). Italicized numbers indicate that the ΔF/F traces in the samples (type II) are mostly intermittent. Student's t tests were performed against WT control of the same frequency in 0.1 mM Ca²⁺ concentration (*p < 0.05, **p < 0.01, ***p < 0.001) or in 0.5 mM Ca²⁺ (+p < 0.05, ++p < 0.01, +++p < 0.001).

rons. Homozygous stocks were first constructed to carry several combinations of the particular Gal4 driver and UAS-GCaMP responder. For instance, a fly strain carrying UAS-GCaMP1.3 (a gift from Dr. Yalin Wang and Dr. Yi Zhong of Cold Spring Harbor Laboratory; cf. Wang et al., 2004; Ueda and Wu, 2006) was recombined with a motor-neuron expressing Gal4 driver P{GawB}c164 (Torroja et al., 1999), forming a fly strain +; c164Gal4-UAS-GCaMP1.3 (referred to as c164-GCaMP1.3). Similarly, UAS-GCaMP6m (Bloomington stock center; Chen et al., 2013) was recombined with *nsynaptobrevin-Gal4* (*nSyb-Gal4*, a gift from Dr. Toshihiro Kitamoto, University of Iowa), forming the strain +; +; *nSyb-GCaMP6m*.

Both c164-GCaMP1.3 and *nSyb-GCaMP6m* were then used to cross with mutants of Na⁺ and K⁺ channels genes, e.g., mutants of the *Sh* K⁺ channel (Jan et al., 1977; Wu and Haugland, 1985; Haugland and Wu, 1990), i.e., ortholog of K_v1 (Iverson et al., 1988; Pongs et al., 1988; Schwarz et al., 1988; Timpe et al., 1988a,b), the *eag* K⁺ channel (Kaplan and Trout, 1969; Ganetzky and Wu, 1983), i.e., EAG (K_v10, Warmke et al., 1991), and the *para* Na⁺ channel (Suzuki et al., 1971), i.e., Na_v1 (Loughney et al., 1989).

For the c164-GCaMP1.3 line, chromosome was then crossed with an attached-X chromosome stock to create the stably maintained strain X^X/+/Y; c164-GCaMP1.3 to generate lines carrying the various mutant alleles of the X-linked Na⁺ and K⁺ channel genes. Male larvae in this attached-X stock, +/Y; c164-GCaMP1.3 served as the wild-type (WT) control. The mutant genotypes include: i. *Sh^M/Y*; c164-GCaMP1.3, ii. *eag¹/Y*; c164-GCaMP1.3, iii. *eag¹ Sh¹²⁰/Y*; c164-GCaMP1.3, iv. *para^{bss1}/Y*; c164-GCaMP1.3, v. *para^{ts1}/Y*; c164-GCaMP1.3. Additional alleles of these genes have been examined to confirm consistent mutational effects, including *Sh¹²⁰* and double mutant *para^{bss1} Sh¹²⁰* (see Results; Table 1).

For *nSyb-GCaMP6m*, virgins of the above *Sh*, *eag* alleles were crossed with male *nSyb-GCaMP6m* to generate *Sh^M/Y*; +; *nSyb-GCaMP6m*/+ and *eag¹/Y*; +; *nSyb-GCaMP6m*/+. RNAi knockdown of *Shab* (*y¹ sc^{*} v¹ sev²¹; P{TRiP.HMS02400}attP40*, Bloomington stock center, see Butler et al., 1989; Tsunoda and Salkoff, 1995; Singh and Singh, 1999; Ueda and Wu, 2006; Peng and Wu, 2007, about *Shab*) was also tested with *nSyb-GCaMP6m*, as specified in figure legends.

The above baseline study were then complemented with additional GCaMP versions, including UAS-GCaMP6f (Chen et al., 2013) and UAS-*myrGCaMP5* (Melom and Littleton, 2013; Melom et al., 2013), as well as an additional Gal4 driver *w*; P{GawB}386Y (Wong et al., 2012; Walker et al., 2013). See further details in Results.

Solutions and preparation

Wandering 3rd instar male larvae were collected from culture bottles and dissected in HL3 saline, containing: 70 mM NaCl, 5 mM KCl, 20 mM MgCl₂, 10 mM NaHCO₃, 5 mM trehalose, and 155 mM sucrose; buffered at pH 7.2 with 5 mM HEPES (Stewart et al., 1994). For optical imaging and electrophysiological recording, the saline was replaced with HL3.1 (70 mM NaCl, 5 mM KCl, 4 mM MgCl₂, 10 mM NaHCO₃, 5 mM trehalose, 115 mM sucrose, and 5 mM HEPES; at pH 7.2) for reliable detection of the distinct excitability defects previously reported for the Na⁺ and K⁺ mutants (Feng et al., 2004; Ueda and Wu, 2006; Lee et al., 2008). For high pH experiments, Tris (pK_a 8.1) was used to replace HEPES in the HL3.1 saline, and the final pH was adjusted with NaOH to 8.8 or 9.8 as specified (Lnenicka et al., 2006). Imaging experiments were performed with saline containing 0.1 mM or 0.5 mM Ca²⁺, as specified. Approximate 5-min equilibration was allowed before stimulation. Ca²⁺ concentration as low as 0.1 mM effectively suppressed muscle contraction, except the occasional occurrence seen in hyperexcitable

mutants, e.g., *eag Sh*. Data contaminated with contractions were excluded from further analysis. In experiments with 0.5 mM Ca^{2+} , sodium glutamate (7 mM) was added for glutamate receptor desensitization and thus suppression of muscle contraction, a common practice to avoid movement artifacts (Macleod et al., 2002; Reiff et al., 2005; Lnenicka et al., 2006). All of the above chemicals were obtained from Sigma-Aldrich.

Ca^{2+} imaging

An upright fluorescent microscope (Eclipse E600FN; Nikon) equipped with a 40 \times water-immersion objective lens (Fluoro; N.A. 0.80) and Nomarski optics was used to visualize synaptic boutons. The light source was a xenon short arc lamp (UJL-75XE; Ushio), filtered by a GFP filter set (excitation filter: 450/50 nm; dichroic mirror: 480 nm; barrier filter: 510/50 nm). Image capture and recording was conducted with the RedshirtImaging NEUROCCD-SM256 system, which includes a CCD camera by Sci-Measure Analytical Systems, and the data acquisition control system (Redshirt Imaging). Data compilation and first-order analyses were performed by using the computer software NeuroPlex of the NEUROCCD-SM256 system, which collects both fluorescent images and electrophysiological signals. The digital images (256 \times 256 pixels per frame) were sampled at a frame rate of 25 Hz.

The larval segmental nerve bundles were severed from the ventral ganglion. The nerve innervating the hemisegment monitored for fluorescence was stimulated using a glass suction electrode (~ 10 μm in diameter, filled with HL3.1). A second suction electrode (7–8 μm , filled with HL3.1), together with an AC amplifier (GRASS model p15, Warwick, RI), was employed to record resulting action potentials and to determine the stimulation threshold (Wu et al., 1978; Ganetzky and Wu, 1982a), which was usually between 1.5 and 2 V with a stimulus duration of 0.1 ms. The stimulation voltage was set to 4–6 V to ensure action potential initiation.

A GRASS S88 stimulator driven by a programmable pulse generator Master-8 (A.M.P.I.) was used to apply the stimulation protocols. In experiments with 0.1 mM Ca^{2+} , 2-, 10-, 20-, 40-, and sometimes 80-Hz stimulation trains (duration 2 s, stimulus pulse width 0.1 ms) were applied sequentially with an inter-trial interval of 4 s (~ 2 min for 40- or 80-Hz stimulation). In the experiments with 0.5 mM Ca^{2+} , the preparations were first stimulated at 1-Hz for 10 s, followed by 2-s trains of 2-, 5-, 10-, 20-, and 40-Hz stimulation.

Simultaneous Ca^{2+} imaging and electrical recording

Simultaneous electrophysiological recordings of either nerve action potentials or extracellular focal excitatory junction potentials (efEJP) were sometimes performed during GCaMP Ca^{2+} imaging. A glass electrode (7- to 10- μm opening, filled with HL3.1, 0.1 mM Ca^{2+} and an inserted AgCl-Ag wire) was used for en passant recording of nerve action potentials, as described above, and for efEJP recording, in which the shank of the electrode was heated and bent (~ 45 – 60°). This enabled the electrode tip to approach the muscle surface underneath the objective lens with a steeper angle to form a loose patch covering

one to two synaptic boutons (Renger et al., 2000; Ueda and Wu, 2009a, 2012). As demonstrated in Fatt and Katz (1952), extracellular recordings of miniature end-plate potentials (mEPPs) follow the faster time course of miniature end-plate currents (mEPCs) as compared to mEPPs and the registered amplitude is proportional to the local mEPCs as determined by the seal resistance between the electrode tip and muscle membrane (leakage to ground). Signals were recorded with the low and high cutoff frequencies set at 0.1 Hz and 50 kHz and fed to the BNC ports of the NEUROCCD-SM256 system. The digitized signals were processed and stored in a PC computer together with the optical data collected at the same time.

Pharmacology

Preparations were examined with the standard stimulation protocol in 0.1 mM- Ca^{2+} HL3.1 to obtain control data and subsequently to determine the effects of 4-aminopyridine (4-AP; Sigma-Aldrich), quinidine (Sigma) or tetraethylammonium (TEA; Eastman Kodak). Measured volumes (1–10 μl) of 4-AP, quinidine or TEA stock solutions were added to the bath (~ 1 ml) to achieve a final concentration of 200 μM for 4-AP, 20 μM for quinidine, 10 or 20 mM for TEA, or mixtures of these drugs as specified. Gentle pipetting ensured even mixture of the bath solution.

The effects of inhibiting mitochondrial proton gradient was studied with the proton ionophore DNP (Kodak). Dissected larval preparations were first imaged in HL3.1 (0.1 mM Ca^{2+}) to obtain control data and the saline was then replaced with HL3.1 containing DNP (0.1 or 0.2 mM, as specified). The effect of DNP incubation was monitored up to 60 min. Sodium azide (NaN_3 ; Fisher Scientific), which inhibits the complex VI of electron-transport chain (Bowler et al., 2006), was also tested (1 mM in HL3.1, 0.1 mM Ca^{2+} ; pH 7.2) using the same protocol.

Mitochondrial staining

GCaMP-expressing larvae were incubated in HL3.1 saline (0.1 mM Ca^{2+}) containing 100 nM tetramethylrhodamine (TMRM; AnaSpec) for 5 min before washing off. An epifluorescence microscope (Eclipse E600FN; Nikon) equipped with a 60 \times water-immersion lens (Fluoro; N.A. 1.00) was used to collect images from both green (GCaMP) and red (TMRM) channels. GCaMP and TMRM images collected from the same fields were manually merged for optimal superposition of boutons and mitochondria. A custom-made python code was used to threshold the green and red channels separately so as to remove the background and selectively outline boutons and strongly-stained mitochondria.

Data analysis and statistics

In each larval preparation, data were collected from one or two axonal terminal branches that innervate muscles 12 and 13. For each branch, 3–10 boutons were sampled. Fluorescence intensity at any time point (F_t) for a bouton was calculated by subtracting the background fluorescence intensity from the bouton fluorescence. The background fluorescence was determined from a selected homogeneous region adjacent to the selected bouton.

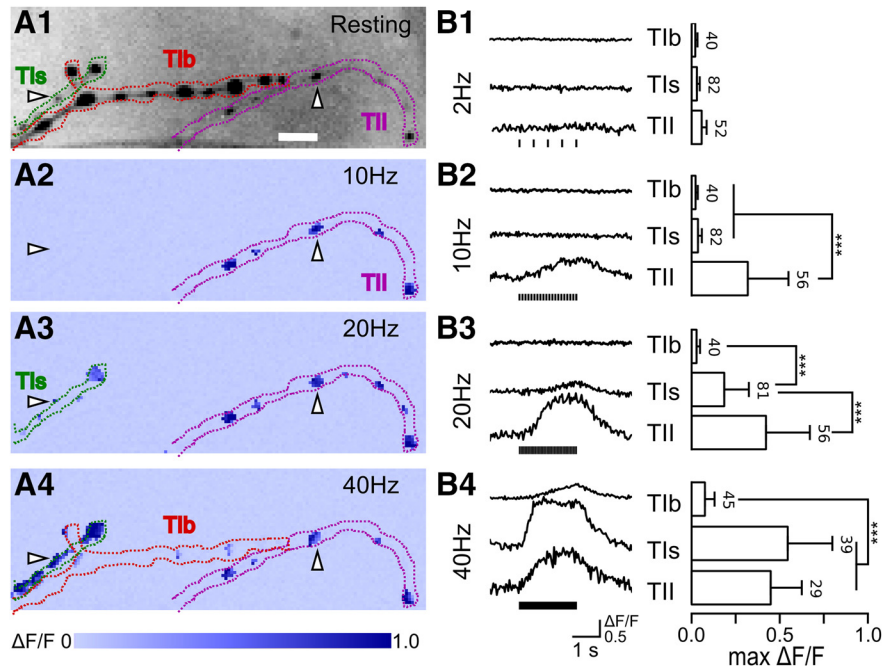


Figure 1. Distinct frequency responses of the GCaMP signals in type Ib, Is, and II synapses. **A1**, Inverted-gray image showing the typical morphology of GCaMP expressing type Ib, Is, and II synaptic terminals in muscle 12. Their contours are traced in red, green, and purple, respectively. Arrowheads indicate a type II bouton (right) and a type Is bouton (left). **A2–A4**, Pseudo-color maps of maximum change in $\Delta F/F$ ($\max \Delta F/F$) under 10-, 20-, and 40-Hz stimulation, respectively. Arrowheads and terminal contours are carried over from **A1**. **B1–B4**, left panels, Representative fluorescence $\Delta F/F$ traces and the corresponding right panels show summary bar plots of $\max \Delta F/F$ for type Ib, Is, and II synaptic boutons from 8–11 NMJs at 2, 10, 20, and 40 Hz, respectively. The vertical scale bar indicates $\Delta F/F$ of 0.5 unit, i.e., 50% increase in fluorescence intensity. Error bars indicate SDs with numbers of boutons indicated. KW tests with Bonferroni corrections were performed. Asterisks indicate highly significant differences; $***p < 0.001$. Ca^{2+} indicator GCaMP1.3 was used in this and the majority of the following figures, except for **Figures 3, 5, 6, 8**. These samples are included in the analysis of a greater data set presented in **Table 1**.

After background subtraction, baseline fluorescence (F_B) was calculated from the mean of the read-out in the 25 frames (1-s duration) before the beginning of stimulation. The values of $\Delta F/F$ were calculated from $(F_t - F_B)/F_B$. The maximum $\Delta F/F$ ($\max \Delta F/F$) within the 2-s window following the onset of stimulation was determined following a 5-point running average of the traces collected. The root mean square of the baseline was calculated to indicate the basal noise level (N_B). Traces with low baseline expression (F_B) or unusually large noise levels (N_B) were excluded from analysis (<5% in total). A bouton was considered nonresponding unless the $\max \Delta F/F$ exceeded 200% of the N_B . Nonresponding boutons were excluded from kinetics analysis.

The half-rise time ($t_{1/2\text{Rise}}$) in kinetic analysis was determined as the time from the onset of stimulation to 50% of the peak value ($\max \Delta F/F$) and the half-decay time ($t_{1/2\text{Decay}}$) the time period between the end of stimulation and the time point where the signal declined to 50%. (Some mutant larvae showed intermittent Ca^{2+} accumulation, and thus $\max \Delta F/F$ did not always correspond to the end of stimulation.) All calculations, plots, and pseudo-color maps were constructed with computer programs written with Numpy and Matplotlib packages in Python language (available on request).

Means and SEMs of data grouped by NMJs are shown in all figures, except for **Figure 1**, where means and SDs of

all boutons for each type of synaptic terminals are shown to indicate the extent of variability. In addition, means and SDs for all datasets are reported in **Tables 1–3**. For datasets that are normally distributed, either *t* test or one-way ANOVA and Fisher’s LSD *post hoc* tests are used to determine significant differences between means. Data sets that failed to pass the normality tests, were subjected to Kruskal–Wallis (KW) tests with Bonferroni corrections for statistical differences (as specified in figure legends and **Tables 1–3**, as well as in the statistics table, **Table 4**). Statistic tests were performed using OriginPro 9.0 made by OriginLab (<http://www.originlab.com>), Microsoft Excel or custom-made python code.

Results

Distinct frequency responses of GCaMP Ca^{2+} signals in glutamatergic type Ib, Is, and aminergic type II synapses

We performed a comprehensive Ca^{2+} imaging analysis by targeted expression of GCaMP indicators in the larval NMJ and found striking differences in the ionotropic glutamatergic type Ib (tonic) and type Is (phasic), and metabotropic octopaminergic type II synapses. Most Ca^{2+} imaging studies have used abdominal muscles 6 and 7 (Macleod et al., 2002; Reiff et al., 2005; Lnenicka et al., 2006), which are innervated by types Ib and Is, but

not by type II, motor axon terminals. We instead chose muscles 12 and 13 as the primary regions of interest. These two muscles are innervated by all three types of synapses, which are individually identifiable by distinct synaptic bouton sizes and terminal branches (Fig. 1A1), as shown previously in immunostaining studies (Johansen et al., 1989; Budnik et al., 1990; Kurdyak et al., 1994; Monastirioti et al., 1995; Zhong and Wu, 2004; Koon et al., 2011). Type Ib, Is, and II axonal terminals each represent the projection from a different motor neuron. Notably, the phasic type Is synaptic terminals in muscles 6, 7, 12, and 13 are derived from separate axonal branches of a single motor neuron (MNSNb/D-Is; Hoang and Chiba, 2001; see also Lnenicka and Keshishian, 2000), whereas muscles 12 and 13 share the same type II motor neuron input (MNSNb/D-II; Hoang and Chiba, 2001; see also Schmid et al., 1999). However, the tonic type Ib motor terminals in muscle 12 and 13 are separately innervated by different motor neurons (MN12-Ib and MN13-Ib; Hoang and Chiba, 2001).

The motor patterns found in *Drosophila* larval NMJs usually consist of trains of high-frequency repetitive action potentials (Budnik et al., 1990; Cattaert and Birman, 2001; Fox et al., 2006; Chouhan et al., 2010). To explore how axonal firing frequency determines the GCaMP Ca^{2+} signals in different synaptic boutons, we applied 2-s trains of repetitive stimuli to the motor axons at increasing frequencies (2, 10, 20, and 40 Hz), which are within the normal range of firing rates of type Ib and Is motor axons (Cattaert and Birman, 2001; Chouhan et al., 2010).

We used HL3.1 saline (Feng et al., 2004; Ueda and Wu, 2006) to optimize the expression of the well characterized excitability mutant phenotypes while retaining a desirable property of the HL3 saline (Stewart et al., 1994) of promoting the longevity of the NMJ preparation. Except for some experiments examining Ca^{2+} dependence, the majority of experiments were conducted with saline containing 0.1 mM Ca^{2+} , which not only could enhance the hyperexcitable mutant phenotypes but also effectively suppressed muscle contraction during imaging (cf. Ueda and Wu, 2009a,b; Ueda and Wu, 2015). This approach also circumvented the use of high-concentration glutamate for postsynaptic receptor desensitization to suppress muscle contraction during imaging (Macleod et al., 2002, 2004, 2006; Lnenicka et al., 2006) and thus minimized potential complications from activating presynaptic metabotropic glutamate receptors (Zhang et al., 1999).

At low frequencies of nerve stimulation (e.g., 2 Hz), we did not detect any significant GCaMP Ca^{2+} signals ($\Delta F/F$) in WT larvae (Fig. 1B1). With 10-Hz stimulation, only type II synapses displayed GCaMP signals (see the pseudocolor map in Fig. 1A2, and example traces with bar graphs in Fig. 1B2). GCaMP signals appeared in type I synapses only at higher stimulation frequencies, above 20 Hz for type Is synapses (Fig. 1A3,B3) and beyond 40 Hz for type Ib synapses (Fig. 1A4,B4).

The distinct frequency responses of GCaMP Ca^{2+} signals in type Ib, Is, and II boutons described above apparently reflect intrinsic differences in synaptic properties and are also evident for NMJs in other ventral and dorsal

muscles examined. As demonstrated in Figure 1A, despite the large variations in size and fluorescence intensity (Fig. 1A1), the boutons along the same terminal branch behaved relatively uniformly (Fig. 1A2–A4) and consistent in the general wave form (see representative traces in Fig. 1B1–B4), so that clear distinction in the threshold of frequency responses could be established among each type II, Is, and Ib motor terminals. More detailed morphometric analyses of Ca^{2+} fluorescent signals demonstrate that the characteristic frequency responses of type Ib, Is, and II synapses were independent of and could not be attributed to differences in basal GCaMP expression levels or synaptic bouton sizes (Xing and Wu, 2016).

We found that the distinction in frequency responses among type Ib, Is, and II synapses remained at higher Ca^{2+} concentrations (with 7 mM glutamate in HL3.1 to suppress muscle contraction; Macleod et al., 2004), with the same sequence of responsiveness to various stimulation frequencies. As shown in Figure 2, at 0.5 mM external Ca^{2+} , type Ib synapses remained to be the least responsive and type II the most responsive (20 Hz for type Ib and 2 Hz for type II; Fig. 2B,D), despite the overall enhanced fluorescent signals compared to 0.1 mM Ca^{2+} (Fig. 1B1–B4). Consistently, the data also indicate that saturation levels of GCaMP signals were reached at different frequencies for three types of boutons (at 0.5 mM Ca^{2+} , 10 Hz for type II, ~ 40 Hz for type Is, and well above 40 Hz for type Ib; Fig. 2B,D).

The relative differences in GCaMP signal frequency responses remained unaltered for the various GCaMP indicators with different sensitivity and subcellular localization. Importantly, as Figure 3 shows, similar distinctions in frequency responses were obtained among the three synaptic types with myrGCaMP5 (Melom and Littleton, 2013; dissociation constant $K_d = 447$ nM, Akerboom et al., 2012), GCaMP6m ($K_d = 167$ nM; Chen et al., 2013), and GCaMP1.3 ($K_d = 234$ nM; Nakai et al., 2001), despite their differences in affinity and sensitivity. Additional indicator GCaMP6f and the Gal4 driver c386Y produced the same frequency responses. In particular, MyrGCaMP5, which is localized to plasma membrane (Melom and Littleton, 2013), still produced the same frequency response differences, suggesting that surface-volume ratio differences among type Ib, Is, and II synaptic boutons did not significantly contribute to their distinct GCaMP signal frequency dependencies, which was consistent with previous report on mammalian neurons (Mao et al., 2008).

Differential excitability control of residual Ca^{2+} dynamics by K^+ channels in type Ib, Is, and II synapses

Previous work has shown that neuronal hyperexcitability caused by mutations or drug blockage of the various K^+ channels could lead to greatly enhanced transmitter release often associated with different patterns of repetitive firing of axonal action potentials at *Drosophila* larval NMJs (Ganetzky and Wu, 1982a, 1983, 1985; Ueda and Wu, 2006). Since GCaMP Ca^{2+} imaging enabled detection at a subcellular resolution to indicate variations in excitability properties among the three categories of syn-

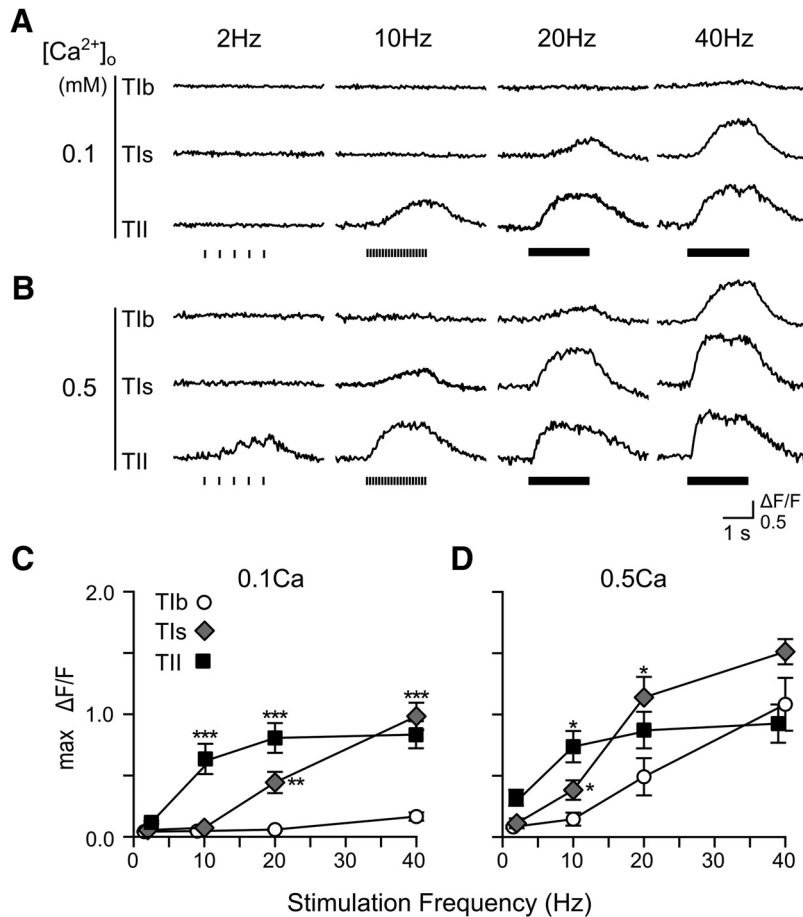


Figure 2. Frequency responses of GCaMP1.3 Ca²⁺ signals at different extracellular Ca²⁺ concentrations. **A, B**, Example ΔF/F traces for type Ib, Is, and II synaptic boutons stimulated at 2, 10, 20, and 40 Hz in 0.1 and 0.5 mM Ca²⁺ saline. **C, D**, Summary line plots showing the frequency responses of averaged max ΔF/F for type Ib, Is, and II synapses at 0.1 mM Ca²⁺ (**C**; 8–11 NMJs, same set of data as in Fig. 1 replotted for comparison) and 0.5 mM Ca²⁺ (**D**; four NMJs). In this and Figures 4, 10, 13, for each NMJ, one synaptic terminal was measured for each type of motor synapses and readings of all boutons within the same terminal were averaged. See Table 1 for total bouton numbers and corresponding NMJ numbers. For clarity, some data points are displaced horizontally and statistically significant differences against type Ib synapses are indicated at each stimulus frequency. In this figure and Figures 4, 10, 13, 14, error bars indicate SEM. Asterisks denote levels of statistically significant differences (**p* < 0.05; ***p* < 0.01; ****p* < 0.001), based on KW tests and Bonferroni correction.

apses, we examined the effects of altering specific K⁺ channels pharmacologically. The differentiation power was further enhanced by systematic analyses of mutants of identified K⁺ channels (Table 1).

TEA and 4-AP are two well-characterized, commonly used K⁺ channel blockers known to cause neuronal hyperexcitability in *Drosophila* NMJs (Jan et al., 1977; Ganetzky and Wu, 1983, 1985; Fox et al., 2005; Ueda and Wu, 2006), as well as other species (Thesleff, 1980; Hille, 2001). Both TEA (10 mM) and 4-AP (200 μM) treatments shifted the frequency responses so that substantial GCaMP Ca²⁺ signals appeared at lower stimulus frequencies (Table 1, compare WT with 4-AP and TEA rows). However, as shown in Figure 4, striking preferential effects were apparent, with TEA strongly enhancing GCaMP signals in type II (at frequencies as low as 2 Hz; Fig. 4A,B) and 4-AP greatly increasing that in type Is synapses (10 Hz; Fig. 4C,D). For type Ib synapses, the effects of TEA and 4-AP were milder and only evident at high stimulation frequen-

cies (above 40 Hz; Table 1). Notably, *Sh* mutations (*Sh^M*, null allele, *Sh¹²⁰*, point mutation) and 4-AP closely resemble in their differential effects on type Ib, Is, and II synapses (Fig. 4; Table 1), consistent with the fact that 4-AP specifically blocks the *Sh* K_v1 channels that mediate fast-inactivating transient K⁺ current I_A in muscle (Salkoff and Wyman, 1983; Wu and Haugland, 1985). Unlike 4-AP, TEA has a different and wider spectrum of action on several types of K⁺ channels at tens of millimolar concentrations (Koketsu, 1958; MacKinnon and Yellen, 1990; Hille, 2001). The contrasting preferential effects of 4-AP on type Is and TEA on type II raise the possibility of different K⁺ channel compositions in type Ib, Is, and II synapses.

One of the most striking demonstrations of extreme hyperexcitability in *Drosophila* NMJs can be seen in *eag Sh* double mutants, in which axon bundles display high-frequency (~100 Hz) repetitive firing of supernumerary action potentials triggered by just one nerve stimulus (Ganetzky and Wu, 1982a, 1983, 1985; Wu et al., 1983).

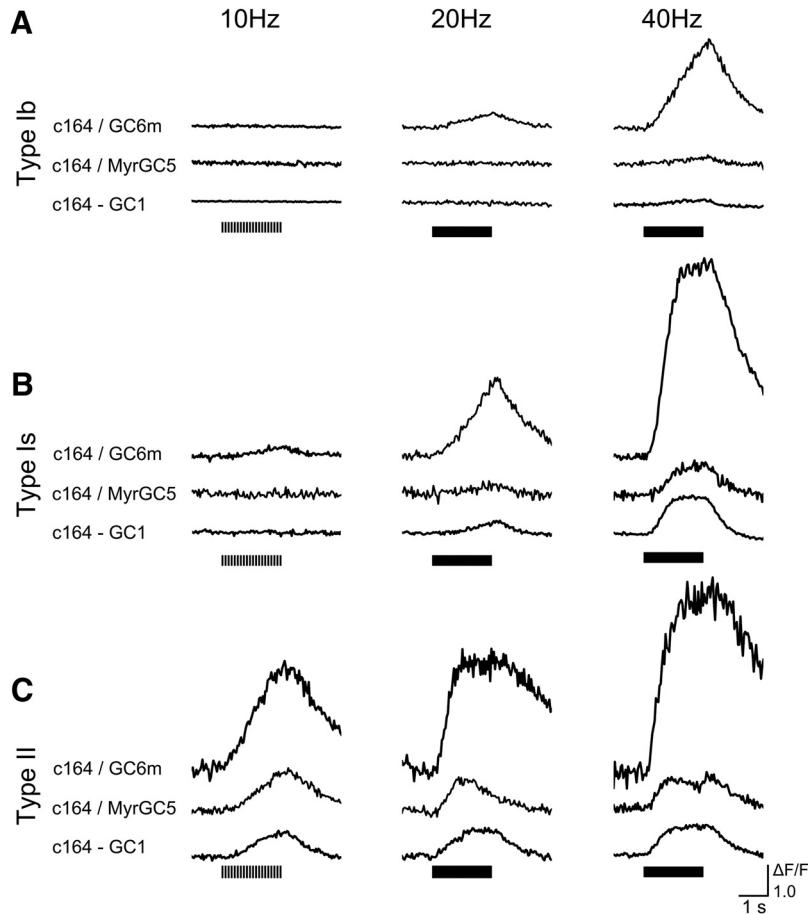


Figure 3. Signals generated by GCaMP indicators of different sensitivity and subcellular localization in response to 10-, 20-, and 40-Hz stimulation. **A–C**, Example $\Delta F/F$ traces for type Ib, Is, and II synaptic boutons recorded with different indicators, c164/GC6m, c164/myrGC5, and c164-GC1 (standing for genotypes: *c164-Gal4/UAS-GCaMP6m*, *c164-Gal4/+; UAS-myrGCaMP5/+* and *+/+; c164-GCaMP1.3*), in 0.1 mM Ca^{2+} saline at the designated stimulation frequencies. Consistently, GCaMP signals of type II synapses appeared in the lowest and type Ib the highest stimulus frequency ranges, regardless of the indicator types.

However, it has not been resolved how type Is and Ib terminals each contributes to this extreme phenotype. As shown in Figure 4, in the double-mutant *eag¹ Sh¹²⁰*, type Is was clearly the most drastically affected, since robust single stimulus-evoked GCaMP signals could be observed only in type Is, but not Ib, synapses (Fig. 4A, 2 Hz), and could not be seen in either *Sh* or *eag* single mutants (Table 1). Enhanced GCaMP signals in type Ib were seen only when stimulated beyond 40 Hz (Table 1, first column) while type II synapses only occasionally displayed single stimulus-evoked responses (see further details below). Taken together, these observations demonstrate type Is motor axon activities as the source of the supernumerary repetitive axonal action potentials in *eag Sh* double mutants and support the notion of different combinations of K^+ channel subtypes in type Ib, Is, and II synapses.

To extend the above findings based on GCaMP1.3 measurements, we performed a separate set of experiments with GCaMP6m, an improved version of GCaMP with increased sensitivity (compare Fig. 3), for a more systematic analysis of the distinctions in K^+ channel functioning among type Ib, Is, and II synapses (Figs. 5, 6).

For the ease of comparisons, representative traces of GCaMP6 responses to 2-, 10-, and 20-Hz stimulation are superimposed for each genotype and condition. For the cases of altered type II synapses, mutations of *eag* channels, as well as *ShabRNAi* knockdown or quinidine (abbreviated as Q in all figures) inhibition of *Shab* K_v2 channels (Singh and Wu, 1989; Wu et al., 1989; Singh and Singh, 1999; Ueda and Wu, 2006), led to clearly discernable GCaMP responses to individual nerve stimuli delivered at 2 Hz in HL3.1 saline containing 0.1 mM Ca^{2+} (Fig. 5; 2-Hz traces). Even more robust effects were obtained with TEA treatment, which has a broad-spectrum action and can act on *Shab* and *eag* channels (Pak et al., 1991; Brüggemann et al., 1993). However, type II synaptic GCaMP signals were less affected by *Sh* mutations or 4-AP treatment, consistent with the GCaMP1.3 results (Fig. 4; Table 1).

In comparison, type Is synapses were most strongly influenced by manipulations of *Sh* channels, with some small GCaMP responses to individual stimuli in the 2-Hz stimulus train detectable in *Sh* or 4AP-treated WT NMJs (Fig. 5, middle column). For type Ib synapses, however,

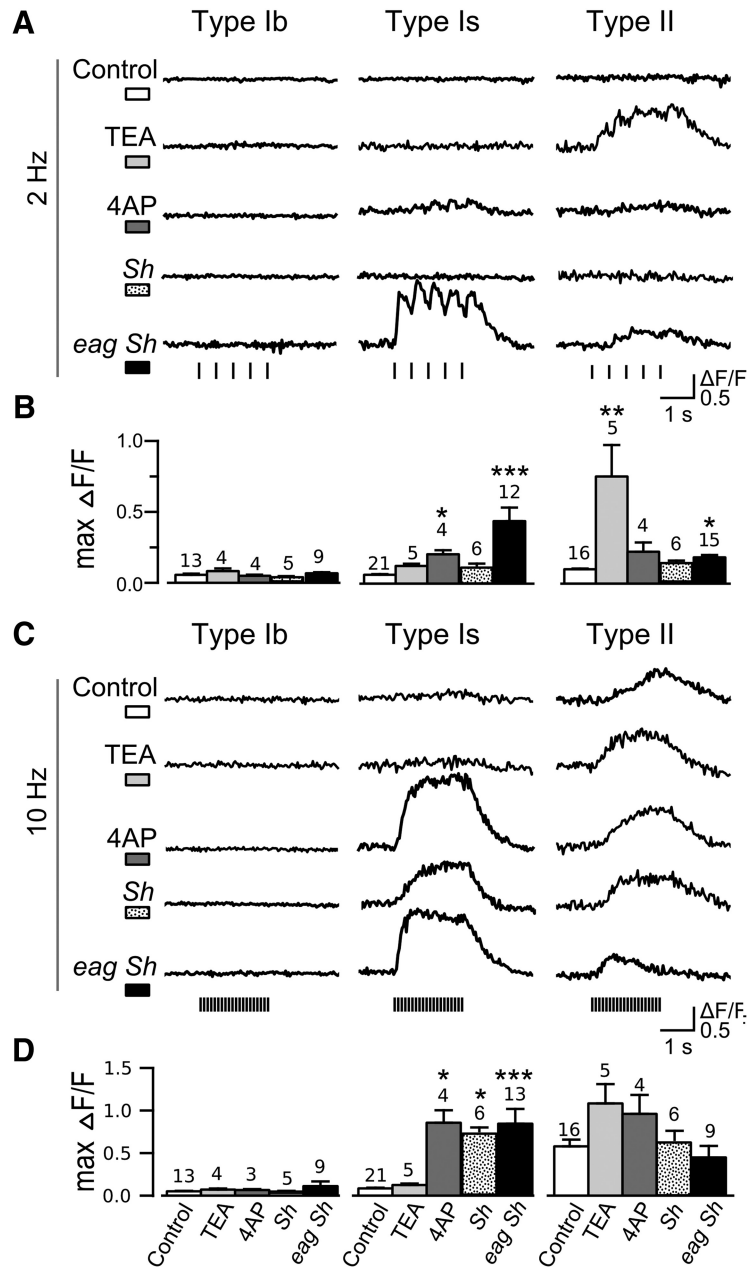


Figure 4. Genetic and pharmacological dissection of the distinct excitability of type Ib, Is, and II synapses. Representative $\Delta F/F$ traces under 2- and 10-Hz stimulations (**A, C**), comparing WT control, WT with TEA (10 mM) and 4-AP (200 μ M) treatments, *Sh^M* mutant and double mutant *eag¹ Sh⁷²⁰*. Note the preferential effects of TEA on type II, and 4-AP, *Sh^M* and *eag¹ Sh⁷²⁰* on type Is synapses. **B, D**, Bar charts for sample statistics corresponding to the traces in **A, C**, with NMJ numbers and SEMs indicated. KW tests with Bonferroni correction were performed; * $p < 0.05$, ** $p < 0.01$, *** $p < 0.001$.

none of the above genetic or pharmacological manipulations was effective in producing GCaMP responses with stimulus frequencies below 20 Hz (Fig. 5, middle column). These GCaMP6m observations confirm the conclusions drawn from the experiments based on GCaMP1 (Fig. 4; Table 1) regarding the differential excitability control of by K^+ channels in type Ib, Is, and II synapses. Taken together, it could be seen that type II synapses were most sensitive to manipulations of *eag* and *Shab* channels, whereas type Is synapses appeared to be particularly vulnerable to disruptions of *Sh* channels, and

type Ib synapses were most resistant to K^+ channel perturbations.

Extreme hyperexcitability and motor terminal repetitive firing

Apparently, a ceiling effect of hyperexcitability is indicated by the robust responses to individual stimuli (delivered in the 2-Hz nerve stimulation), as seen in TEA-treated type II synapses (Fig. 5, right column). We found that type Is synapses could also reach this ceiling effect at 0.1 mM Ca^{2+} but only after double insults of the combined per-

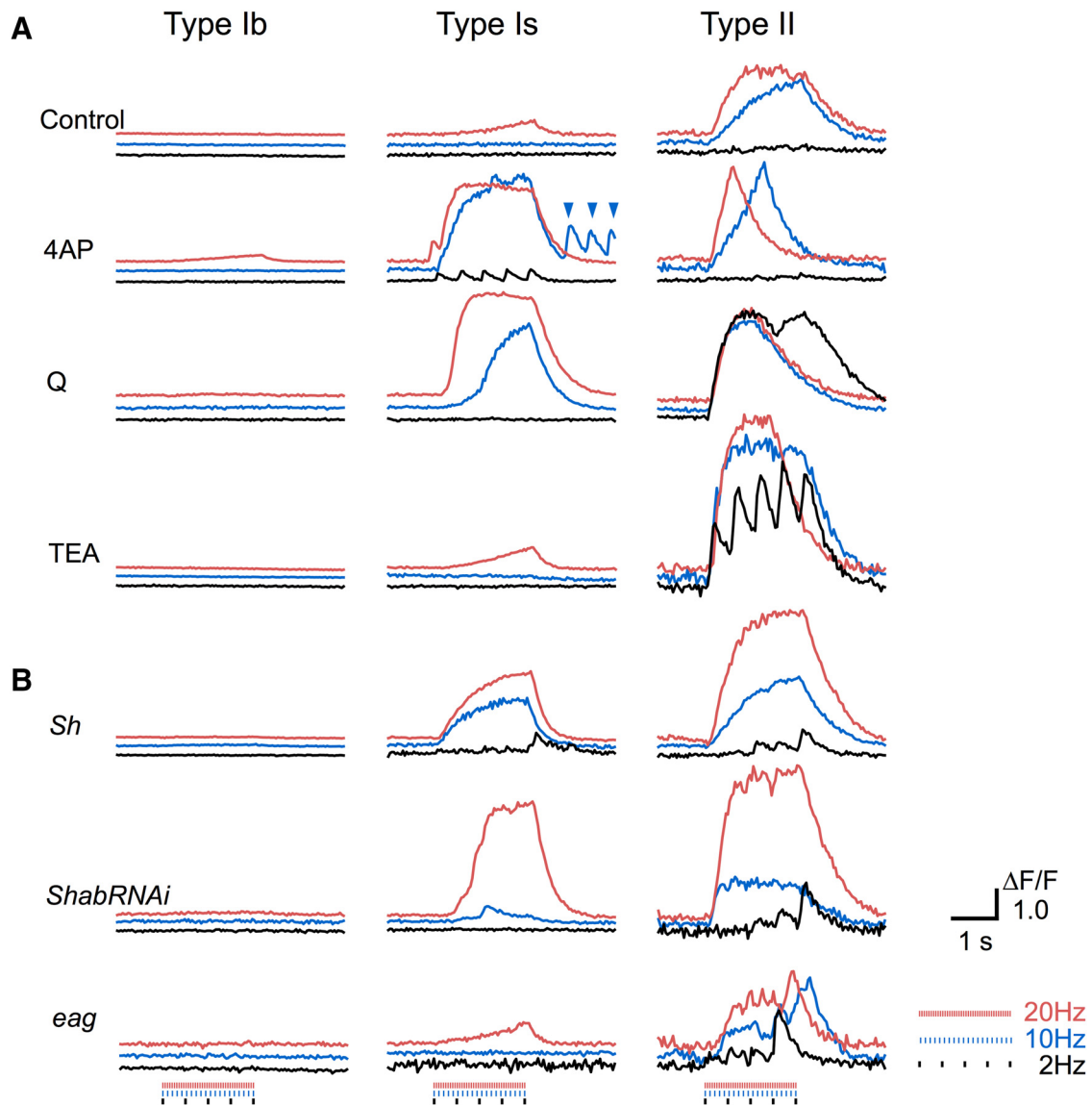


Figure 5. Distinct effects of various genetic and pharmacological perturbations of K⁺ channels on type Ib, Is, and II synapses at different stimulus frequencies. Note that these perturbations preferentially lowered the frequency threshold for GCaMP signals in type Ib, Is, and II synapses. **A**, +; +; *nSyb-GCaMP6m* larvae used as WT control (0.1 mM Ca²⁺, top-row traces), examined by applying 4-AP (200 μM), quinidine (abbreviated as Q, 20 μM), and TEA (10 mM). Black trace, 2-Hz stimulation; blue, 10 Hz; red, 20 Hz. Note the drastic frequency response change in type II synapses (2 Hz, Q and TEA), in type Is (10 Hz, 4-AP), and in type Ib (20 Hz, 4-AP). **B**, Genetic perturbation of GCaMP signals examined with *Sh^{M/Y}*; *nSyb-GCaMP6m/+*, *eag^{1/Y}*; +; *nSyb-GCaMP6m/+*, and *UAS-ShabRNAi/+*; *nSyb-GCaMP6m/+*. Three to five larvae for each condition were tested and consistent results were obtained.

turbations of *Sh* with either *eag* or *Shab* channels. Similar to the GCaMP1 results of *eag Sh* double mutants (Fig. 4), greatly enhanced GCaMP6m signals in response to individual nerve stimuli could be seen in type Is synapses by the joint effects of 4AP (or *Sh* mutations) with either quinidine (or *ShabRNAi*) or TEA (Fig. 6A, middle column, 2-Hz traces).

In contrast, type Ib synapses remained largely nonresponsive at 2 Hz during the above double perturbations (Fig. 6A, left column). It required at least 10 Hz for type Ib synapses to exhibit clearly detectable GCaMP signals even with both *Sh* and *Shab* channels disrupted (Fig. 6A; for single perturbation results, see Table 1; Fig. 5). How-

ever, type Ib synapses could display the hallmark of hyperexcitability if given the condition of triple insults with mutations or blockers of K⁺ channels. With triple insults, i.e., combinations of TEA and 4AP (or *Sh*) plus quinidine (or *ShabRNAi*), type Ib synapses exhibited single pulse-evoked robust GCaMP signals in 0.1 mM Ca²⁺ saline (Fig. 6B, left column, 2-Hz traces), directly comparable to the ceiling level of hyperexcitability found in type Is and type II synapses (Figs. 5, 6A). Therefore, compared to type II and Is synapses, type Ib synapses appeared to possess a greater K⁺ channel-mediated repolarization capacity and were hence more resilient to disruptions in different types of K⁺ channels.

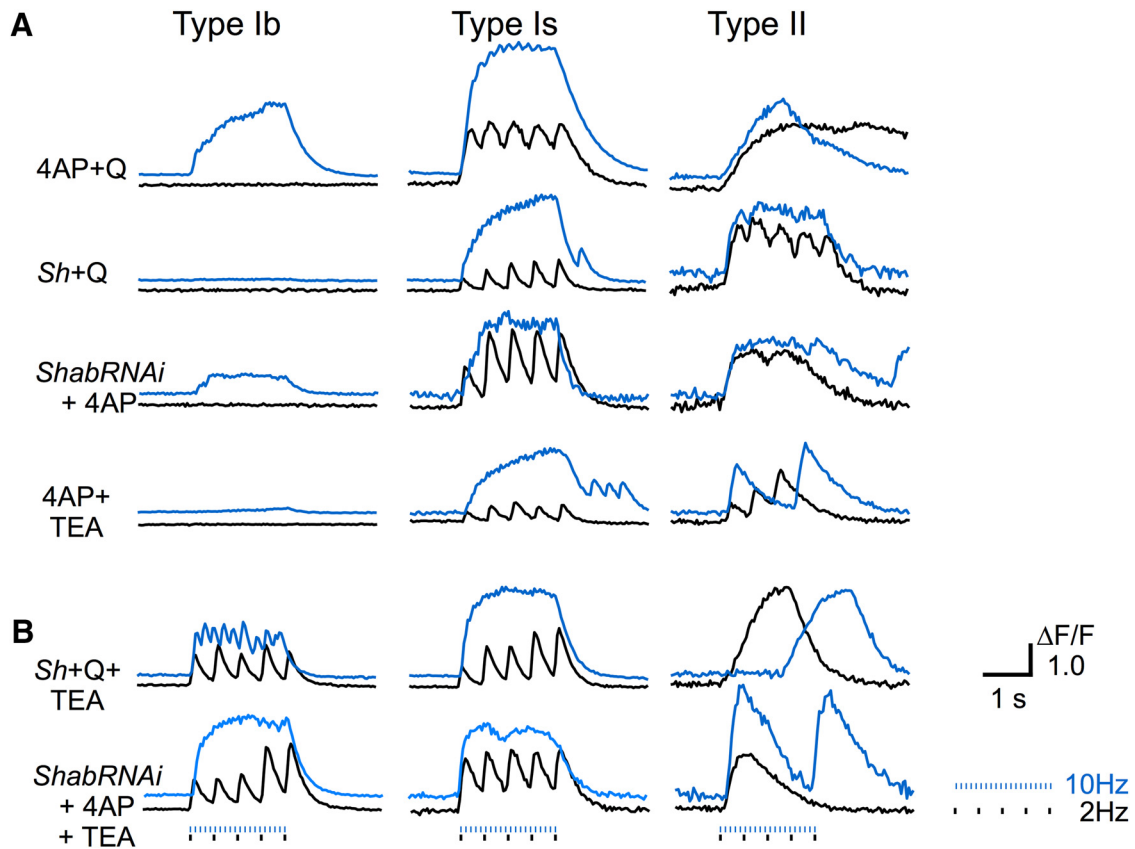


Figure 6. Extreme excitability indicated by single pulse-evoked giant GCaMP signals: double and triple insults of combined mutation and drug effects. GCaMP6m signals ($\Delta F/F$) in response to 2-Hz (black) and 10-Hz (blue) stimulation from larvae carrying the *nSyb-GCaMP6m* construct (0.1 mM Ca^{2+}). *nSyb-GCaMP6m*, used as WT control (0.1 mM Ca^{2+}), examined by coapplication **A**, Double insults of combined effects of 4-AP (200 μM) + quinidine (Q, 20 μM), *Sh^M* + quinidine (20 μM), *ShabRNAi* + 4-AP (200 μM), and 4-AP (200 μM) + TEA (10 mM). Note the robust GCaMP signals in type II and Is synapses evoked by individual stimuli (2 Hz) and the preferential response of type Ib synapses to combined insults of 4-AP + Q or *ShabRNAi* (10 Hz). **B**, Triple insults of K^+ channel perturbations with *Sh^M* + Q (20 μM) + TEA (10 mM), or *ShabRNAi* + 4-AP (200 μM) + TEA (10 mM). Note the single pulse-evoked giant GCaMP signals in type Ib synapses (2 Hz), indicating a state near the ceiling effect of hyperexcitability. Also note that hyperexcitability resulted in interrupted, aborted or rebounding GCaMP signals in type II synapses (2 and 10 Hz) and rebounds of type Is responses (10 Hz). Based on observations from three to five larvae for each condition.

To understand how the modified GCaMP signals were correlated with the amplitude and frequency of the synaptic transmission events, we performed simultaneous focal recording in conjunction with GCaMP imaging on the same synaptic boutons. efEJPs follow the faster time course of excitatory junctional currents (EJCs) as compared to EJPs and their amplitudes are linearly proportional to the local EJCs generated by the synaptic release in region under the electrode tip (Fatt and Katz, 1952; Sakmann and Neher, 1984). This approach enabled a direct correlation of postsynaptic response induced by transmitter release with the presynaptic GCaMP signals triggered by nerve stimulation. At low external Ca^{2+} (0.1 mM), both type Ib and Is produced only small efEJP responses at a level of quantal fluctuation in WT larvae and there were no detectable signals from GCaMP1.3 and GCaMP6m indicators (Figs. 7, 8). However, we found both GCaMP1.3 and GCaMP6m indicators were unable to produce detectable signals even when efEJPs were clearly discernable. For example, type Ib and Is bou-

tons in *Sh* larvae (Fig. 7), or in WT following 4-AP and quinidine treatment (Fig. 8), produced greatly enhanced efEJPs that were not registered by either GCaMP1.3 or GCaMP6m.

A notable exception was during the robust 2-Hz peaks of GCaMP6 signals (the hallmark hyperexcitability ceiling effect) in type Is synapses at low external Ca^{2+} (0.1 mM) after double insults of K^+ channels, such as application of 4-AP plus quinidine, where giant efEJPs occurred in correlation with each GCaMP $\Delta F/F$ peak (Fig. 8, right column; compare Fig. 6, middle column). A closer examination of these highly nonlinear events revealed that these efEJPs consisted of massive discharge of multiple release of transmitters (expanded type Is efEJP traces in Fig. 8; and also Fig. 9 for *eag Sh* double mutant effect). Further investigation with triple recordings to correlate axonal action potentials with efEJP and GCaMP signals demonstrated that these massive efEJP discharges underlying individual GCaMP $\Delta F/F$ peak were evoked by high-frequency supernumerary firing of motor axons (~100 Hz; Fig. 9).

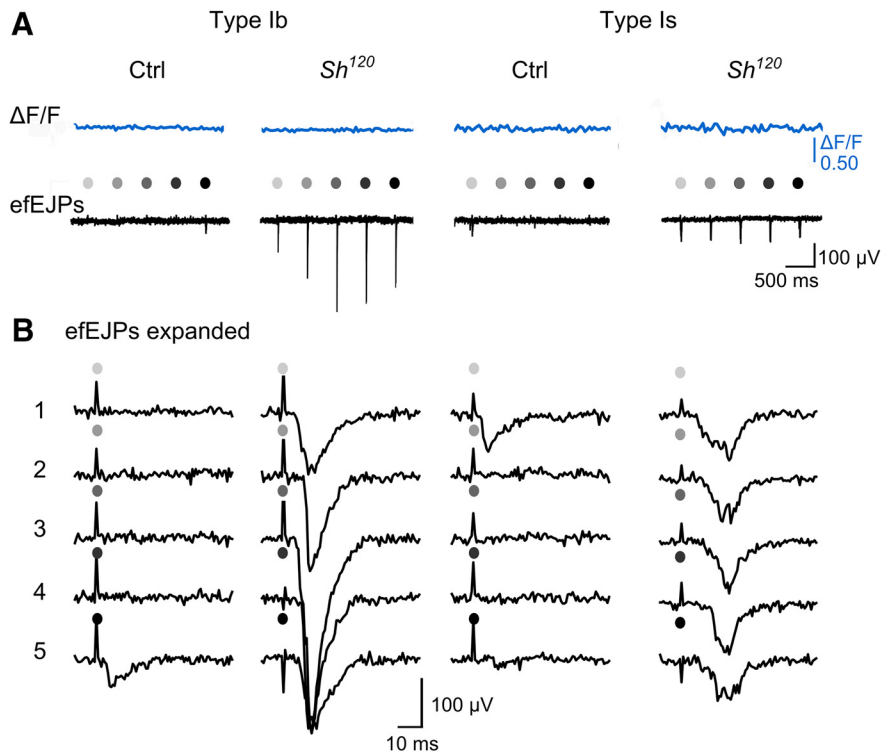


Figure 7. Failure to detect presynaptic GCaMP signals when synaptic transmission events were registered by efEJPs. **A**, Traces of GCaMP1.3 $\Delta F/F$ (blue) and efEJPs (black) at 2-Hz stimulation collected from the same boutons of type Ib and Is motor terminals of WT control (*c164-GCaMP1.3*) and *Sh*¹²⁰/*γ*; *c164-GCaMP1.3*. Each stimulus is indicated by a gray-scaled dot. **B**, Expanded traces of efEJPs in response to the sequential stimuli that are shown in **A**. Note that no detectable GCaMP signals (**A**) despite significant transmissions (**B**).

It is important to note that in all of the experiments reported here, the segmental nerve was severed from the ventral ganglia. Therefore, the repetitive action potentials were generated within the axon and were not driven by CNS activities mediated by the motor neurons. Thus, these hallmark, ceiling effects of GCaMP signals reflect axonal membrane hyperexcitability and are consistent with previous reports of multiple firing of motor axons associated with prolonged, giant EJPs at low external Ca^{2+} levels found in *eag Sh* (Ganetzky and Wu, 1982a) and *Sh Shab* (Ueda and Wu, 2006) double mutants.

Differential effects of Na⁺ channel mutations on GCaMP signals and nerve conduction failure in type II motor axons

The above observations reveal distinct repolarization mechanisms of the three synaptic terminals, presumably reflecting differential expression of K⁺ channel genes. We found similarly disparate sensitivities to Na⁺ channel mutations among the three types of synapses, although in *Drosophila para* is the only known gene that encodes voltage-gated Na⁺ channel (Na_v1), which regenerates a large number of splice variants (Loughney et al., 1989; Thackeray and Ganetzky, 1994; Olson et al., 2008; Lin et al., 2012). To investigate the role of the Na⁺ channel, we took advantage of two well-characterized *para* alleles that confer drastic but opposite effects on the membrane depolarization mechanism. The hypoexcitable, temperature-

sensitive allele *para*^{ts1} is thought to decrease the synthesis of functional Na⁺ channels (Thackeray and Ganetzky, 1994), resulting in increased axonal refractory period and higher sensitivity to Na⁺ channel-specific toxins (Wu and Ganetzky, 1980; Suzuki and Wu, 1984), and becomes paralyzed at high temperature due to axonal conduction failure (Suzuki et al., 1971; Siddiqi and Benzer, 1976; Ganetzky et al., 1986). In contrast, the hyperexcitable, bang-sensitive allele *bss1* displays seizure behaviors on mechanical stress (Ganetzky and Wu, 1982b; Burg and Wu, 2012), which is associated with seizure-like nerve spike discharges in central circuits (Lee and Wu, 2006; Parker et al., 2011) and increased synaptic transmission with axonal multiple firing at the larval NMJ (Ganetzky and Wu, 1982b; Giachello and Baines, 2015).

The GCaMP1 imaging demonstrated that like *Sh* K⁺ channel mutations, the hyperexcitable *para* allele *bss1* had a strong preferential effect on type Is over Ib synapses (Fig. 10A, 10 and 20 Hz; Table 1). Notably, GCaMP signals were significantly enhanced in type Is boutons on stimulation at 10 and 20 Hz, whereas little effect on type Ib synapses was detectable up to 40 Hz. This preferential effect again raises the possibility of differential expression or posttranslational modifications of Na⁺ channel splice isoforms (Thackeray and Ganetzky, 1994; Olson et al., 2008; Lin et al., 2012). However, the *bss* effect on type Ib could be revealed once combined with *Sh*¹²⁰ since the double mutant

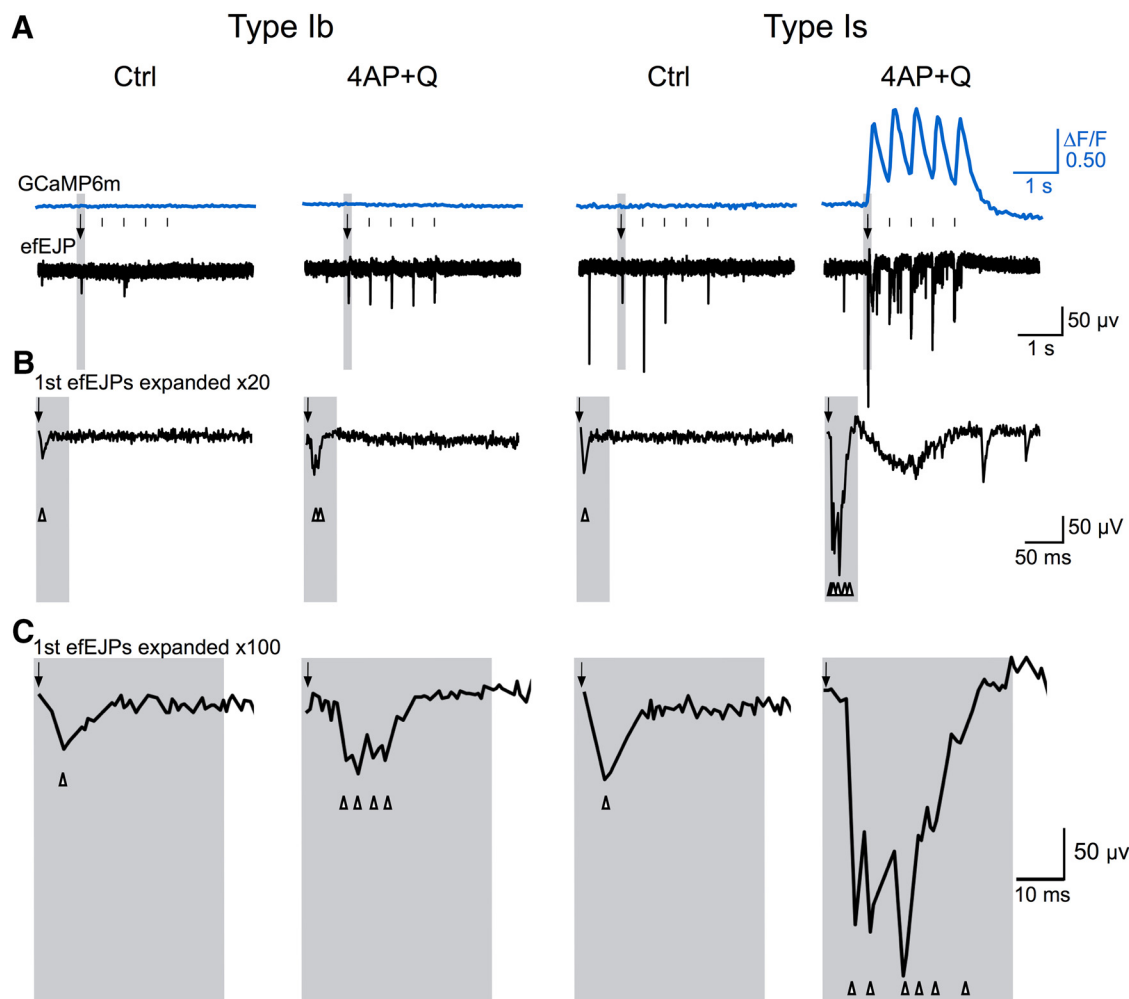


Figure 8. Correlation of giant GCaMP signals with repetitive efEJPs evoked by individual stimuli. **A**, $\Delta F/F$ signals of the GCaMP6m indicator correlated with simultaneous focal recording of efEJPs from the same boutons in type Ib and Is motor terminals (2-Hz stimulation in 0.1 mM Ca^{2+} HL3.1 saline). K^+ channel blockade with 4-AP (200 μM) and quinidine (Q, 20 μM) in *nSyb-GCaMP6m* larvae led to giant GCaMP signals in type Is, but not Ib, synapses. Expanded efEJP traces (20 and 100 times, shaded time windows) in **B**, **C** indicate supernumerary transmitter releases (arrowheads) following each nerve stimulus (arrow).

produced much larger response than either single mutant alone (Table 1). On the contrary, in both type Ib and Is synapses, the hypoexcitable temperature-sensitive *para* allele *ts1* produced only small, but statistically significant, reductions in the GCaMP signals at room temperature (Table 1; Fig. 10A).

In comparison, type II synapses in both *ts1* and *bss1* alleles produced more striking, clear-cut alterations. The hypoexcitable *ts1* mutation results in significantly smaller GCaMP signals in type II synapses even at room temperature (10 and 20 Hz; Fig. 10B). Notably, a significant fraction of the stimulation trials produced no response at all (20-Hz sample trace in Fig. 10B), indicating axonal conduction failure. This lowered safety margin for action potential propagation in the type II motor axons could be explained by the higher longitudinal internal resistance for axons with smaller diameters (Aidley, 1998), making them more vulnerable to the effect of reduced density or modified function in Na^+ channel that determine the depolarizing Na^+ current across the plasma membrane. Such

axonal conduction failure was not observed in the larger type Ib or Is motor terminals in *para^{ts1}* NMJs. For the hyperexcitable allele *bss1*, a striking nonlinear frequency response was illustrated by the GCaMP signals in type II synapses. Greatly enhanced GCaMP signals were seen at 2 Hz, with discernable responses to individual stimuli (compare type II, 2-Hz traces in Figs. 5, 10B). However, at increased stimulus frequencies a suppression of GCaMP responses was seen, concurrently with a novel, unexpected pattern of interrupted or aborted GCaMP signals. These events occurred in the rising phase of GCaMP signals during repetitive stimulation (Fig. 11), resulting in a net decrease in the average Max $\Delta F/F$ in *bss1* (Fig. 10B, plot, 20–40 Hz). Boutons of the same type II synaptic terminal in the same NMJ behaved uniformly in the interrupted or aborted pattern, with the timing and kinetics entirely the same. Such seemingly puzzling GCaMP responses suggest intermittent axonal AP conduction failure at increasing stimulus frequencies.

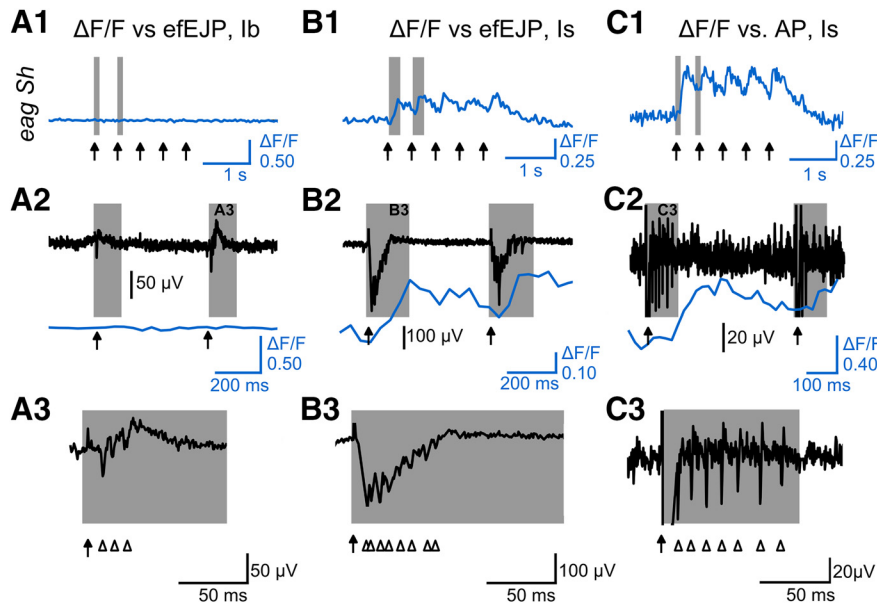


Figure 9. Electrophysiological basis of single pulse-evoked giant GCaMP signals: repetitive firing due to extreme hyperexcitability of the motor axon. GCaMP signals ($\Delta F/F$ traces) of type Ib (**A1**) and Is (**B1**, **C1**) synapses from three *eag¹ Sh^{120/Y}; c164-GCaMP1.3* larvae at 2-Hz stimulation in 0.1 mM Ca^{2+} HL3.1 saline. Corresponding simultaneous records of efEJPs (**A2**, **B2**) and nerve action potentials (**C2**) are displayed in black with the associated $\Delta F/F$ traces in blue (expanded from **A1**, **B1**, **C1** with individual nerve stimuli marked by arrows). One of the two shaded areas in **A2**, **B2**, **C2** are further expanded to show efEJPs with multiple peaks (arrowheads), indicative of repetitive nerve action potentials, which were more robust in type Is than Ib synapses (**A3**, **B3**). En passant nerve recording revealed motor axon high-frequency repetitive firing (over 100 Hz; **C3**).

It has been shown that in the oocyte expression system, *para^{bss1}* Na^+ channels exhibit slower recovery from inactivation (Parker et al., 2011), which could lengthen action potential refractory period. This would make small-diameter type II axons particularly prone to action potential failure at high stimulation frequencies.

It is important to point out that a similarly phenomenon of interrupted GCaMP signals in type II motor terminals was also found in other hyperexcitable K^+ channel mutants, such as *eag* and *eag Sh* (Fig. 11; see also Fig. 4, *eag¹ Sh¹²⁰* type II, 10 Hz). This apparently counter-intuitive observation in hyperexcitable K^+ channel mutants could also be associated with increased action potential refractory period (cf. *para^{bss1}*), which made the axons nonresponsive to the upcoming stimuli after excessive firing activities. It is known that in *eag¹ Sh¹²⁰* a longer refractory period (Engel and Wu, 1992) results from excessive inactivation of Na^+ channels following over excitation due to weakened repolarizing K^+ currents. As shown in Figures 5, 6, different mutational and drug manipulations of K^+ channels could lead to irregular waveforms of GCaMP6 signals, most pronouncedly in type II synapses. Intermittent, delayed, aborted, or sometimes lost accumulation of the GCaMP signal occurred frequently (Fig. 5, type II 10 and 20 Hz). Following more drastic manipulations (double or triple insults), these irregularities became more extreme, occurring even at 2-Hz stimulation (Fig. 6). Notably, these extreme hyperexcitability conditions also caused GCaMP signal rebound after stimulus cessation, which was encountered more frequently in type II and occasionally in type Is synaptic terminals (Figs. 5, 6).

Differential effects on rise and decay kinetics of alterations in Ca^{2+} influx and clearance

The above irregular waveforms of GCaMP signals reflect either high-frequency axonal repetitive firing or intermittent axonal conduction failure. However, in most cases GCaMP signals registered gradual residual Ca^{2+} accumulation and followed a time course of smooth rise during repetitive stimulation and an approximately exponential decay at the cessation of stimulus trains.

In principle, the GCaMP Ca^{2+} signal reflects an integrated dynamic process of Ca^{2+} influx and subsequent clearance of intracellular free Ca^{2+} . Thus, analysis of the rise and decay kinetics of GCaMP signals may yield further insight into how alterations in membrane excitability can change the time course of intracellular Ca^{2+} accumulation. To visualize the overall GCaMP Ca^{2+} signal rise and decay kinetics in response to repetitive stimulation, $\Delta F/F$ were normalized and overlaid to contrast for changes caused by channel blockers and mutations (Fig. 12; Tables 2, 3). As expected, we found that the rise phase of GCaMP signals was accelerated by acute application of higher external Ca^{2+} concentrations (Fig. 12A), increased stimulus frequencies (Fig. 12B), K^+ channel blockers (Fig. 12C), and mutations that increase membrane excitability (Fig. 12D). All of these manipulations, including 4-AP and TEA treatments as well as *Sh* and *bss1* mutations, resulted in faster GCaMP signals with shortened peaking or plateauing time. All these changes in rise kinetics were indicated by shortened half-rise time, as quantified and summarized in Table 2. Note that the preferential effects of individual channel blockers and mutations on type Ib, Is, and II synapses are again illustrated in the extents of

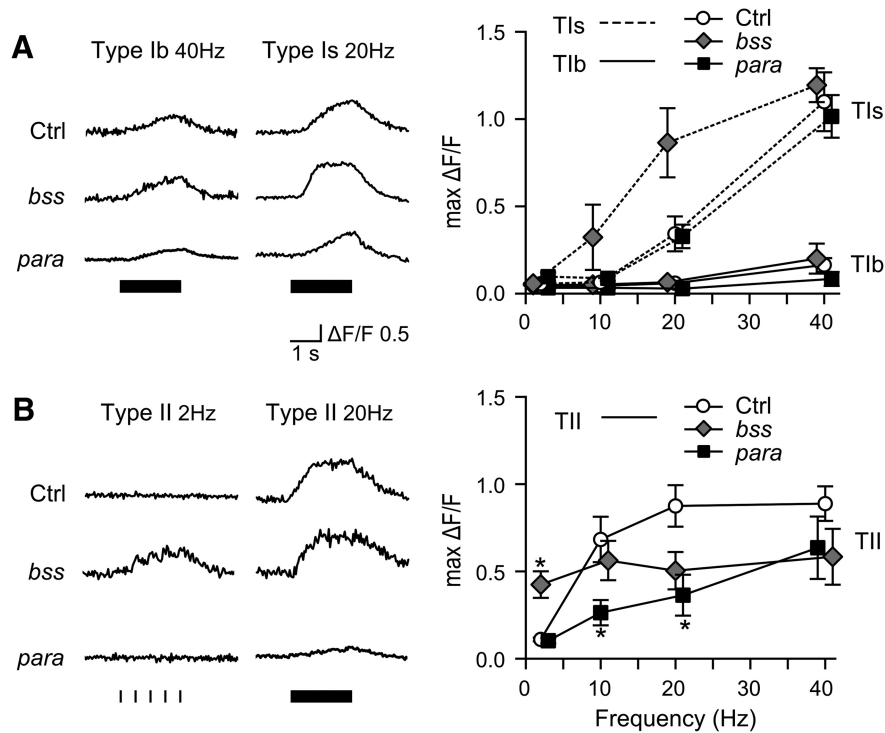


Figure 10. Differential effects of Na⁺ channel mutations on the Ca²⁺ dynamics of type Ib, Is, and II synapses. GCaMP Ca²⁺ signals of type Ib and Is (A) and II (B) NMJs from a hypoexcitable allele, *para*^{ts1} (*para*) and a hyperexcitable allele, *para*^{bss1} (*bss*) are compared, with representative ΔF/F traces at specified frequencies shown in left panels and the corresponding frequency dependence of max ΔF/F in right panels (mean and SEM, of 6–11 NMJs for each genotype, compare Table 1). Note that type II synaptic boutons in *bss* frequently displayed “intermittent” or “aborted” GCaMP signals on repetitive stimulation, lowering the average max ΔF/F above 10 Hz (see Fig. 11 for details). KW ANOVA with Bonferroni corrections were performed (**p* < 0.05, ***p* < 0.01).

rise time acceleration (Fig. 12). Single pulse-evoked GCaMP signals showed even shorter peaking time (Figs. 5, 6), consistent with the high-frequency repetitive firing of action potentials triggered by each stimulus pulse in these cases of hyperexcitability (Fig. 9).

Remarkably, when compared to the half-rise time, the half-decay time of GCaMP signals was much less affected by enhanced membrane excitability (4-AP and TEA in Fig. 12C; *Sh* and *para*^{bss1} in Fig. 12D; compare

Tables 2, 3 for additional genotypes and conditions). This is true also for a higher external Ca²⁺ concentration (0.5 mM; Fig. 12A; Tables 2, 3). These observations apparently reflect an abundant reserve of Ca²⁺ clearance capacities that could still handle the increased influx caused by drug treatments or mutations in our experiments.

However, it should be noted that in extreme hyperexcitability conditions, such as the combined effects of 4-AP, quinidine, and TEA, long-lasting repetitive firing of

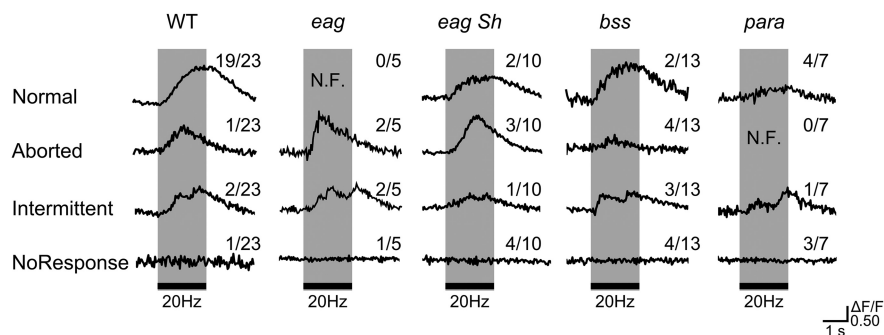


Figure 11. Variability in the wave form of GCaMP signals in type II synaptic terminals at high frequencies of stimulation. Representative regular (normal) and irregular (aborted, intermittent, and no response) ΔF/F traces at 20 Hz from WT, *eag*, *eag Sh*, *bss*, and *para* type II boutons (with *c164-GCaMP1.3*) are shown. For each genotype, the numbers of NMJs exhibiting each wave form are indicated together with the total sample size (numbers of NMJs examined). N.F., not found. Note that both hypoexcitable (*para*^{ts1}) and hyperexcitable (others) mutations increased the occurrence of irregular waveforms, indicating axonal conduction failure in type II motor terminals (see text). Similar response waveforms were also revealed by GCaMP6m indicator (e.g., for *eag*^{1/Y}; *nSyb-GCaMP6m/+*; normal: 0/6, aborted: 2/6, intermittent: 3/6, no response: 1/6).

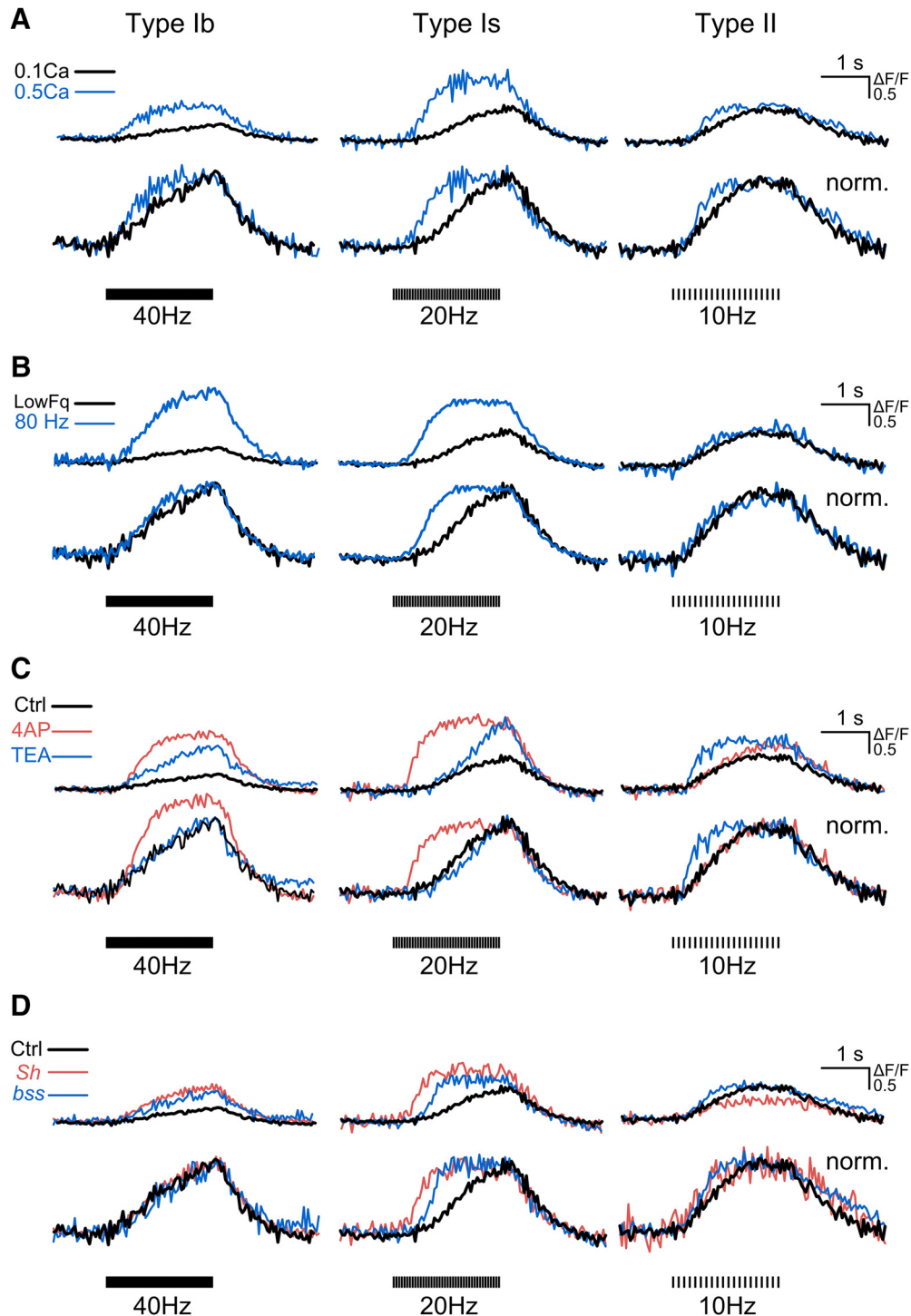


Figure 12. Kinetic analysis of presynaptic GCaMP signals with different manipulations enhancing Ca^{2+} influx. Comparison of original (upper) and normalized (lower) $\Delta F/F$ traces collected from individual boutons of (**A**) WT with 0.1 mM Ca^{2+} (black) versus 0.5 mM Ca^{2+} (blue), (**B**) WT with 0.1 mM Ca^{2+} under the designated stimulation frequency (black, 40 Hz for Ib, 20 Hz for Is, and 10 Hz for II) versus 80-Hz stimulation (blue), and (**C**) WT control (black) versus 4-AP (200 μM , red) and TEA (10 mM, blue) treatments, 0.1 mM Ca^{2+} . **D**, WT control (black) versus *Sh^M* (*Sh*, red), and *bss1* (*bss*, blue). Type Ib, Is, and II synapses, stimulated at 40, 20, and 10 Hz, respectively, in 0.1 mM Ca^{2+} . Note clear alterations in the rise kinetics with minimal effects in the decay kinetics indicated by superimposing normalized traces. See Tables 2, 3 for ensemble data of rise and decay kinetics.

Table 2. Rise kinetics for type I and II synapses of different genotypes

Genotype	Type Ib		Type Is		Type II	
	40 Hz	20 Hz	40 Hz	10 Hz	20 Hz	40 Hz
	$t_{1/2Rise} \pm SD$ (n, N)	$t_{1/2Rise} \pm SD$ (n, N)	$t_{1/2Rise} \pm SD$ (n, N)	$t_{1/2Rise} \pm SD$ (n, N)	$t_{1/2Rise} \pm SD$ (n, N)	$t_{1/2Rise} \pm SD$ (n, N)
0.1 mM Ca²⁺						
WT	1.12 ± 0.26 (18,5)	1.17 ± 0.19 (99, 14)	0.68 ± 0.21 (47, 9)	0.94 ± 0.32 (68, 13)	0.67 ± 0.20 (72, 13)	0.68 ± 0.20 (24, 7)
WT + 4AP	0.66 ± 0.10 (19, 3)***	0.39 ± 0.09 (32, 4)***	0.34 ± 0.17 (29, 3)***	0.76 ± 0.18 (20, 4)***	0.48 ± 0.24 (20, 4)**	0.49 ± 0.32 (21, 3)**
WT + TEA	1.03 ± 0.23 (20, 4)	1.00 ± 0.22 (29, 4)**	0.61 ± 0.13 (25, 4)	0.43 ± 0.27 (15, 5)***	0.55 ± 0.30 (15, 5)*	0.55 ± 0.19 (19, 4)
<i>Sh^M</i>	0.89 ± 0.21 (47, 7)**	0.43 ± 0.12 (81, 9)***	0.39 ± 0.27 (67, 9)***	0.85 ± 0.25 (41, 6)*	0.62 ± 0.16 (43, 6)	0.51 ± 0.22 (29, 6)**
<i>Sh¹²⁰</i>	1.20 ± 0.13 (13, 3)	0.49 ± 0.21 (35, 4)***	0.23 ± 0.14 (23, 4)***	0.89 ± 0.19 (23, 3)*	0.58 ± 0.14 (26, 3)*	N.D.
<i>eag¹</i>	1.10 ± 0.22 (31, 6)	1.12 ± 0.29 (28, 6)	0.64 ± 0.14 (56, 6)	N.A. [†]	N.A. [†]	N.A. [†]
<i>eag¹ Sh¹²⁰</i>	0.78 ± 0.23 (25, 6)***	0.39 ± 0.23 (55, 7)***	0.25 ± 0.13 (46, 5)***	N.A. [†]	N.A. [†]	N.A. [†]
<i>para^{bss1}</i>	1.10 ± 0.18 (39, 9)	0.74 ± 0.38 (65, 9)***	0.63 ± 0.14 (29, 3)	N.A. [†]	N.A. [†]	N.A. [†]
<i>para^{ts1}</i>	1.02 ± 0.26 (6, 3)	1.28 ± 0.19 (26, 5)*	0.75 ± 0.20 (33, 7)	N.A. ^{††}	N.A. ^{††}	0.87 ± 0.31 (20, 3)
<i>para^{bss1} Sh¹²⁰</i>	1.19 ± 0.17 (27, 4)	0.33 ± 0.06 (33, 6)***	N.D.	0.61 ± 0.34 (11, 5)***	0.53 ± 0.16 (22, 6)***	N.D.
0.5 mM Ca²⁺						
WT	0.53 ± 0.19 (25, 4)***	0.57 ± 0.12 (31, 5)***	0.28 ± 0.06 (34, 4)***	0.43 ± 0.17 (33, 5)***	0.36 ± 0.21 (36, 5)***	0.23 ± 0.13 (29, 5)***
<i>Sh¹²⁰</i>	0.62 ± 0.07 (25, 3)	0.33 ± 0.11 (22, 3)++	0.18 ± 0.05 (17, 2)+++	0.52 ± 0.14 (32, 4)++	0.27 ± 0.09 (33, 4)	0.23 ± 0.15 (27, 4)
<i>para^{bss1}</i>	0.69 ± 0.12 (26, 3)++	0.58 ± 0.10 (48, 4)+++	0.25 ± 0.06 (34, 3)	0.28 ± 0.15 (18, 4)+++	0.21 ± 0.09 (19, 4)+++	0.26 ± 0.14 (12, 4)

Data are presented as $t_{1/2Rise} \pm SD$ (n, N), where $t_{1/2Rise}$ indicates half-rise time in seconds. N.A., not applicable, because of intermittent responses (†) or low-amplitude signals masked by baseline noise (††). N.D., not determined. The bolded font indicates significant difference from wild-type control. Student's *t* tests were performed against WT control at the same frequency in 0.1 mM Ca²⁺ (**p* < 0.05, ***p* < 0.01, ****p* < 0.001) or in 0.5 mM Ca²⁺ (+*p* < 0.05, ++*p* < 0.01, +++*p* < 0.001).

action potentials could occur after the end of stimulation (Ganetzky and Wu, 1982a; Ueda and Wu, 2006), which extended the decay time course of GCaMP signals in a manner of “rebound” or oscillation (mostly in type II and sometimes in type Is synapses, see examples in Figs. 5, 6).

In addition to manipulating the factors that regulate Ca²⁺ influx, we also examined known mechanisms affecting Ca²⁺ clearance for indications of their differential actions on type Ib, Is, and II synapses. As previously shown for type Ib synapses, a major Ca²⁺ extrusion mechanism in *Drosophila* NMJ is PMCA (Lnenicka et al., 2006; Klose et al., 2009). The H⁺/Ca²⁺ exchange pump PMCA relies on inward transport of proton counter-ions for Ca²⁺ export, and

can thus be inhibited by high external pH (Niggli and Sigel, 2008). High-pH inhibition of PMCA is effective and has been employed to manipulate Ca²⁺ transients in *Drosophila* NMJ synapses (Lnenicka et al., 2006; Klose et al., 2009; Caldwell et al., 2013), squid giant axon (Dipolo and Beaugé, 1982), and mammalian neurons and pancreatic cells (Benham et al., 1992; Chen et al., 2003).

Following an established protocol, we compared Ca²⁺ extrusion efficacy among the three types of synapses in low and high pH saline (pH 7.2 vs 8.8; cf. Lnenicka et al., 2006). The results showed that acutely increased extracellular pH not only slowed down the decay kinetics as expected (Fig. 13A,B), but could also accelerate the rise

Table 3. Decay kinetics for type I and II synapses of different genotypes

Genotype	Type Ib		Type Is		Type II	
	40 Hz	20 Hz	40 Hz	10 Hz	20 Hz	40 Hz
	$t_{1/2Decay} \pm SD$ (n, N)	$t_{1/2Decay} \pm SD$ (n, N)	$t_{1/2Decay} \pm SD$ (n, N)	$t_{1/2Decay} \pm SD$ (n, N)	$t_{1/2Decay} \pm SD$ (n, N)	$t_{1/2Decay} \pm SD$ (n, N)
0.1 mM Ca²⁺						
WT	0.53 ± 0.19 (18,5)	0.46 ± 0.20 (102, 16)	0.50 ± 0.11 (47, 8)	0.77 ± 0.27 (67, 13)	0.84 ± 0.20 (72, 13)	0.73 ± 0.20 (24, 6)
WT + 4AP	0.52 ± 0.07 (19, 3)	0.48 ± 0.10 (32, 4)	0.53 ± 0.09 (29, 3)	0.85 ± 0.24 (20, 4)	0.74 ± 0.23 (18, 4)	1.07 ± 0.23 (18, 4)***
WT + TEA	0.46 ± 0.10 (17, 4)	0.56 ± 0.23 (29, 4)*	0.56 ± 0.15 (25, 4)	0.64 ± 0.25 (16, 5)	0.64 ± 0.37 (16, 5)	0.88 ± 0.29 (19, 4)
<i>Sh^M</i>	0.40 ± 0.08 (47, 7)*	0.52 ± 0.10 (81, 9)*	0.48 ± 0.11 (67, 8)	0.81 ± 0.25 (37, 6)	0.77 ± 0.39 (29, 6)	0.71 ± 0.25 (21, 6)
<i>Sh¹²⁰</i>	0.40 ± 0.10 (13, 3)	0.56 ± 0.11 (35, 4)*	0.54 ± 0.09 (23, 4)	0.78 ± 0.19 (23, 3)	0.72 ± 0.24 (26, 3)*	N.D.
<i>eag¹</i>	0.58 ± 0.32 (31, 6)	0.47 ± 0.20 (28, 6)	0.60 ± 0.13 (56, 5)*	N.A. [†]	N.A. [†]	N.A. [†]
<i>eag¹ Sh¹²⁰</i>	0.54 ± 0.23 (25, 6)	0.68 ± 0.30 (65, 10)*	0.57 ± 0.20 (46, 5)	N.A. [†]	N.A. [†]	N.A. [†]
<i>para^{bss1}</i>	0.42 ± 0.19 (39, 7)*	0.55 ± 0.09 (58, 7)	0.48 ± 0.09 (29, 6)	N.A. [†]	N.A. [†]	N.A. [†]
<i>para^{ts1}</i>	N.A. ^{††}	0.49 ± 0.20 (26, 5)	0.48 ± 0.13 (33, 7)	N.A. ^{††}	N.A. ^{††}	0.70 ± 0.24 (20, 4)
<i>para^{bss1} Sh¹²⁰</i>	0.64 ± 0.45 (27, 4)	0.50 ± 0.20 (33, 6)	N.D.	0.76 ± 0.23 (18, 6)	0.83 ± 0.36 (22, 6)	N.D.
0.5 mM Ca²⁺						
WT	0.45 ± 0.08 (20, 4)	0.47 ± 0.10 (35, 5)	0.50 ± 0.05 (38, 4)	0.71 ± 0.36 (33, 5)	0.89 ± 0.37 (37, 5)	0.60 ± 0.20 (28, 4)
<i>Sh¹²⁰</i>	0.41 ± 0.09 (25, 3)	0.48 ± 0.09 (22, 3)	0.55 ± 0.10 (17, 2)	0.93 ± 0.25 (32, 4)	0.90 ± 0.36 (33, 4)	0.78 ± 0.34 (27, 4)
<i>para^{bss1}</i>	0.42 ± 0.08 (26, 3)	0.53 ± 0.22 (48, 4)	0.67 ± 0.37 (34, 3)	1.28 ± 0.41 (18, 4)+++	1.31 ± 0.36 (19, 4)+++	1.13 ± 0.57 (12, 4)+++

Data are presented as $t_{1/2Decay} \pm SD$ (n, N), in which $t_{1/2Decay}$ indicates half-decay time in seconds. N.A., not applicable, because of intermittent responses (†) or low-amplitude signals masked by baseline noise (††). N.D., not determined. The bolded font indicates significant difference from wild-type control. Student's *t* tests were performed against WT control at the same frequency in 0.1 mM Ca²⁺ (**p* < 0.05, ***p* < 0.01, ****p* < 0.001) or in 0.5 mM Ca²⁺ (+*p* < 0.05, ++*p* < 0.01, +++*p* < 0.001).

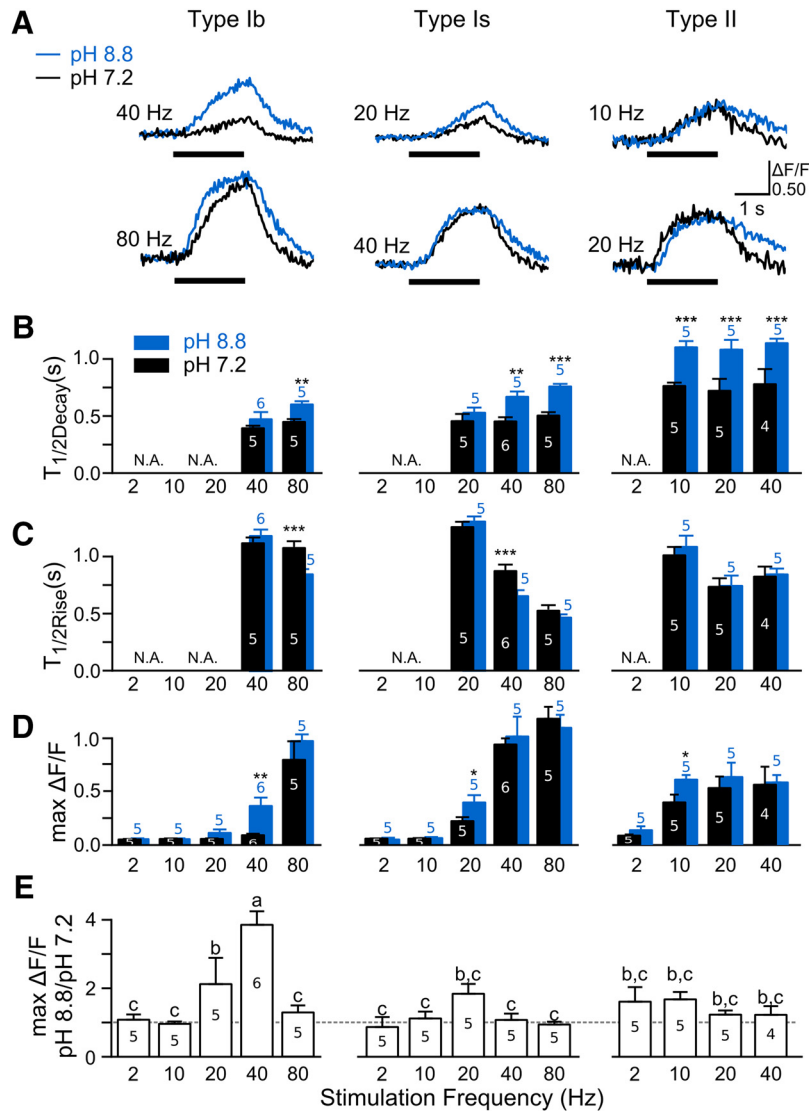


Figure 13. Effects of PMCA inhibition at high pH on Ca^{2+} dynamics of type Ib, Is, and II synapses. **A**, $\Delta\text{F}/\text{F}$ traces of WT larvae in control pH (7.2, black) and high pH (8.8, blue) saline. Overlapping traces from the same individual boutons illustrate the consequences of suppressing plasma membrane Ca^{2+} extrusion via PMCA at a lower (subplateauing, upper row) and a higher (plateauing, lower row) stimulation frequencies. **B–D**, Averaged half-decay time ($T_{1/2\text{Decay}}$), half-rise time ($T_{1/2\text{Rise}}$), and peak GCaMP signals (max $\Delta\text{F}/\text{F}$), respectively, at different stimulation frequencies for type Ib, Is, and II synapses (five to six NMJs from different larvae; N.A., not applicable due to small signals unsuitable for reliable kinetic determination). Statistically significant differences between high and low pH are indicated (t tests; * $p < 0.05$, ** $p < 0.01$, *** $p < 0.001$). **E**, Relative increment in GCaMP signal amplitude determined as the ratio of max $\Delta\text{F}/\text{F}$ between pH 8.8 and 7.2 measurements. One-way ANOVA and Fisher’s LSD tests, a, $p < 0.001$, significantly different from group c; b, $p < 0.05$, significantly different from group c. The dashed line indicates the ratio of 1. Note that PMCA inhibition most effectively increased max $\Delta\text{F}/\text{F}$ around the threshold frequencies (**D**, **E**; i.e., 40, 20, and 10 Hz), coupled with lengthening of decay time above the plateauing frequencies (**B**; i.e., 80, 40, and 10 Hz) for Ib, Is, and II synapses, respectively.

and increase the amplitude of GCaMP signals significantly under some conditions (Fig. 13C–E).

In pH 7.2 saline, the half-decay time of GCaMP1 signals was ~ 0.5 s for both type Ib and Is and ~ 0.7 – 0.8 s for type II synapses at both 0.1 and 0.5 mM Ca^{2+} (Fig. 13B; Table 3; other GCaMP indicators reported similar decay times, compare Fig. 3; data not shown). Immediately on pH increase to 8.8, the half-decay time in both type Ib and Is synapses increased to 0.6–0.7 s (Fig. 13B, 40–80 Hz) while a more pronounced increase to ~ 1.1 s was seen in type II synapses (Fig. 13B, 10–40 Hz).

Compared to retarded decay kinetics, high-pH treatment rendered milder effects, in terms of accelerated rise and enhanced peak amplitude, on GCaMP signals in all three types of synapses. Acceleration of the rise phase was detected somewhere below the “saturation frequency” where GCaMP signals approached the highest attainable amplitude (Fig. 13C, 80 and 40 Hz for type Ib and Is; compare Figs. 2C, 13D, Table 1). It is interesting to note that these were similar to the frequencies at which the lengthening in decay time became evident for type Ib and Is synapses (80 and 40 Hz; Fig. 13B). In contrast,

significant enhancement of amplitude (max $\Delta F/F$) was found around the “threshold frequencies”, where GCaMP signals became readily detectable (Fig. 13C, 40, 20, and 10 Hz for type Ib, Is, and II synapses, respectively), and the relative enhancement (fold change) was greatest in type Ib synapses (Fig. 13D,E, at 40 Hz).

To investigate the extent of involvement of PMCA in synaptic Ca^{2+} clearance, we further increased saline pH to 9.8 and found that pH 9.8 led to greater increases in the decay time of GCaMP signals in all three synapses (>1 s for type I synapses) and shifted GCaMP signals to lower frequency ranges (Ib: 20 Hz, Is: 10 Hz). However, under this condition, the GCaMP signal rapidly ran down within about ten minutes, precluding reliable quantitative determination of the lengthening in half-decay time.

Prolonged mitochondrial inhibition and energy-dependent Ca^{2+} clearance in type Ib, Is, and II synapses

Exporting Ca^{2+} out of cell or into intracellular organelles against its concentration gradient requires energy expenditure, e.g., ATP hydrolysis. Mitochondria are critical for ATP synthesis to power active Ca^{2+} clearance mechanisms such as PMCA, a Ca^{2+} -ATPase (Zenisek and Matthews, 2000; Shutov et al., 2013). A maintained proton gradient across mitochondrial inner membrane is required for these ATP-dependent Ca^{2+} clearance mechanisms, as well as direct mitochondrial sequestration of intracellular free Ca^{2+} (Tang and Zucker, 1997; David et al., 1998; Suzuki et al., 2002).

The proton ionophore DNP is known to reversibly uncouple mitochondrial proton gradient from oxidative phosphorylation (Higgins and Rogers, 1976; Nguyen et al., 1997; Buckler and Vaughan-Jones, 1998; Petrenko et al., 2010). We performed time-lapse measurements of GCaMP signals during the 1-hour DNP treatment. Subsequent to the basal measurements (control, or “0” min; Fig. 14), the preparation was incubated in 0.2 mM DNP saline (0.1 mM Ca^{2+} in HL3.1). Among the three synaptic types, type II synapses first showed drastically lengthened decay time course (20-min incubation; Fig. 14A–D, dark blue traces and bars) in correlation with its slowest basal and high pH decay times among the three (Fig. 13B; Table 3). On further incubation (up to 60 min), drastically prolonged decay times of GCaMP signals were also observed in type Ib and Is synapses, while type II synapse stopped responding to stimulation by this time (Fig. 14A–D, light blue traces and bars). However, further continuous DNP incubation eventually led to total loss of GCaMP responses in all synapses. It is important to note that the lengthened decay time course of individual synaptic terminals was partially reversible, if DNP washout was done before GCaMP response loss. Irreversible loss of GCaMP responses of individual synaptic terminals occurred first in some type II synapses (starting around 20 min into incubation) and then in a smaller portion of type Ib and Is synapses (~ 60 min). Compared to the dramatic alterations in decay kinetics, the rise kinetics, i.e., half-rise time, were only mildly affected by DNP treatment (Fig. 14, compare D, E).

DNP incubation greatly enhanced GCaMP signals of both type Ib and Is synapses so that significantly greater GCaMP signals were observed even at low (10 Hz) stimulation frequencies (Fig. 14A,F, left and middle columns). Such a shift of threshold frequency was most evident in type Ib synapses (from 40 to 10 Hz; Fig. 14F). Notably, DNP effects were further promoted with hyperactivity. It was found that hyperexcitable *eag Sh* accelerated the onset of characteristic DNP effect in type Ib and Is synapses (slower decay and enhanced amplitude) to within 25 min, compared to >40 min in WT. Conceivably, higher activity levels in *eag Sh* could drain the ATP reserve at a faster rate.

A possible effect of long-term proton ionophore (e.g., DNP) treatment is depolarization of the plasma membrane potential (Hodgkin and Keynes, 1955) and thus increased Ca^{2+} influx, as prolonged mitochondrial inhibition leads to diminished ATP supply for Na^+/K^+ ATPase, which maintains the resting membrane potential. However, this effect may not have reached a significant level within the time frame of our experiments, i.e., the repetitive firing as demonstrated by correlating focal recording with GCaMP imaging (compare Figs. 8, 9). Within 1 hr, DNP treatments induced enhanced GCaMP signals with prolonged decay time course, but this was seldom accompanied by supernumerary eEJPs or significant elevation of baseline GCaMP fluorescence (except for 1 out of >10 larvae, excluded from analysis). To obtain a different line of evidence for this striking mitochondrial inhibition effect, we used azide, which inhibits the complex IV in the electron transport chain (Fei et al., 2000). Long-term incubation in azide (1 mM, 60–90 min) resulted in similarly drastic slow decay kinetics of GCaMP6m signals (half-decay time >3 s in all three synapses) and shift in threshold frequency (Ib: from 40 to 20 Hz, Is: from 20 to 10 Hz).

All these lines of evidence indicate that intact mitochondrial metabolism is critical for presynaptic Ca^{2+} clearance, which differs in capacity in type Ib, Is, and II synapses. We therefore examined the mitochondrial density in these synapses by staining the NMJ with TMRM, a fluorescent indicator sequestered into mitochondria by the electrochemical proton gradient (Scaduto and Grotyhann, 1999). By overlaying the mitochondrial staining with GCaMP fluorescence, it was evident that type Ib synapses were most enriched with abundant mitochondria, with 94% of boutons (22 NMJs, four WT larvae, SD = 11%) housing one or more mitochondria (Fig. 15B). type Is synaptic boutons also contained a good amount of strongly-stained mitochondria ($71 \pm 39\%$ of boutons, 21 NMJs, four larvae; Fig. 15B,C), although less than type Ib ($p < 0.05$, t tests with Bonferroni correction). However, type II synaptic boutons rarely contained visible mitochondrial staining ($16 \pm 21\%$, 18 NMJs, four larvae; Fig. 15C), which suggests either significantly less mitochondria availability or lower membrane potential to render TMRM staining of existing mitochondria, or both, than type Ib and Is ($p < 0.001$, t tests with Bonferroni correction). The lower density of active mitochondria in type II synapses correlates well with its slower Ca^{2+} clearance rate (Fig. 13B; Table 3) and higher vulnerability to DNP inhibition (Fig. 14).

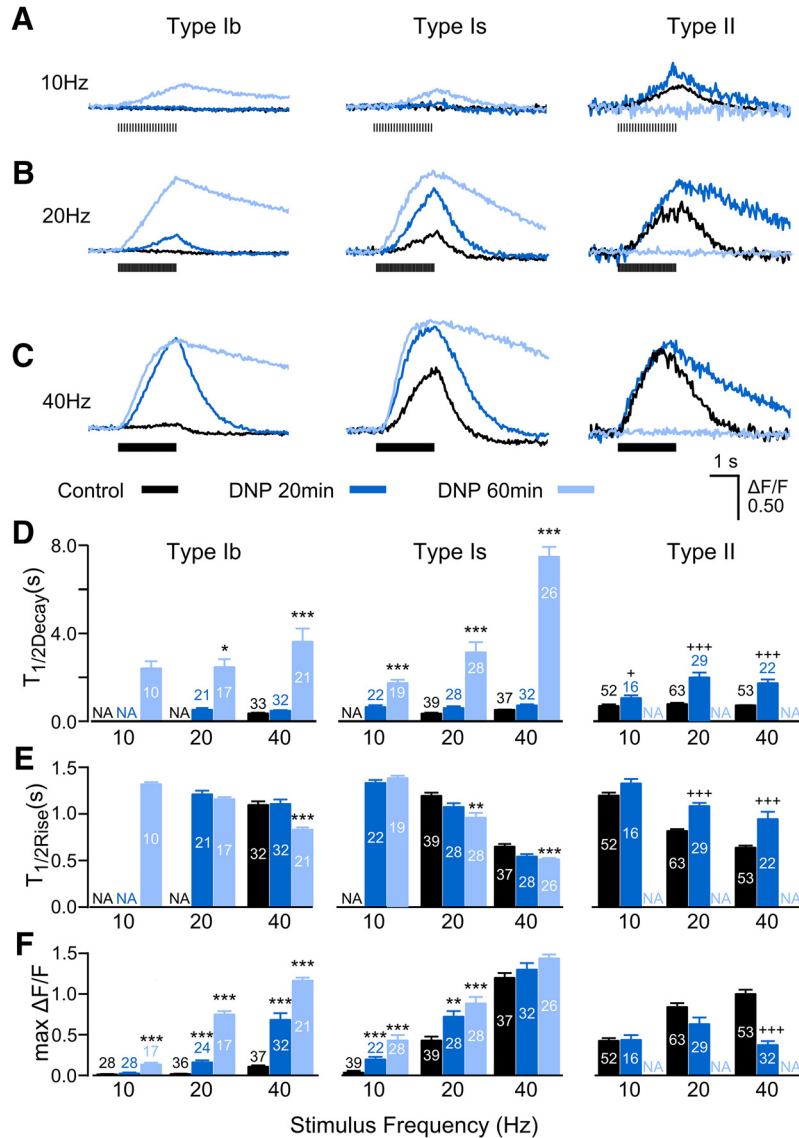


Figure 14. Drastic effects of prolonged DNP treatment on Ca^{2+} dynamics in all three types of synapses. **A–C**, Overlaid representative GCaMP Ca^{2+} signal $\Delta F/F$ traces under 10-, 20-, and 40-Hz stimulation, after 0-, 20-, and 60-min exposure to DNP (black, blue, and light blue, respectively). Note that type II synapses (right column) completely lost responses after a 60-min exposure (light blue), and within a 20-min exposure, about half of type II synapses had already lost responses (data not shown). **D–F**, Summary bar charts for the half-decay time, half-rise time, and maximum $\Delta F/F$ of GCaMP Ca^{2+} signal under 10, 20, and 40 Hz of repetitive stimulation. N.A., not applicable because the corresponding GCaMP $\Delta F/F$ traces were too small or simply nonresponsive to stimulation, thus excluded from kinetic determination (e.g., type II after a 60-min DNP treatment, and type Ib and Is at low stimulation frequencies). Number of boutons (sampled from six different larvae) are indicated. KW tests with Bonferroni corrections were performed among each frequency group; * and $+p < 0.05$, $**p < 0.01$, $***$ and $+++p < 0.001$. For type II synapses after a 20-min DNP treatment, + and +++ denote statistical differences with the dwindling sample sizes due to loss of responses in some type II NMJs after DNP treatment.

Discussion

Genetically encoded GCaMP indicators are widely used for detecting neuronal circuit activities *in vivo*. However, the analytic power of GCaMP signals has not been fully exploited to extract information regarding basic synaptic physiology. In this study, we took advantage of the special anatomic features of the *Drosophila* larval NMJ to contrast properties of metabotropic aminergic (type II) and ionotropic glutamatergic (tonic type Ib and phasic type Is) synapses using several GCaMP Ca^{2+} indicators. Simultaneous monitoring of GCaMP signals from the three synapses within the same microscopic field demonstrates

differential excitability control of Ca^{2+} influx by Na^+ and K^+ channels. Analyses of both kinetic and amplitude features of GCaMP signals reveal the extreme effects of particular Na^+ and K^+ channels on each of the three synaptic types, as well as the prominent roles of mitochondria-powered Ca^{2+} clearance mechanisms in shaping their distinct Ca^{2+} handling properties.

The complex nature of GCaMP signals

We present a summary diagram of how the various genetic and pharmacological manipulations influence Ca^{2+} influx and clearance, hence the amplitude and kinetics of

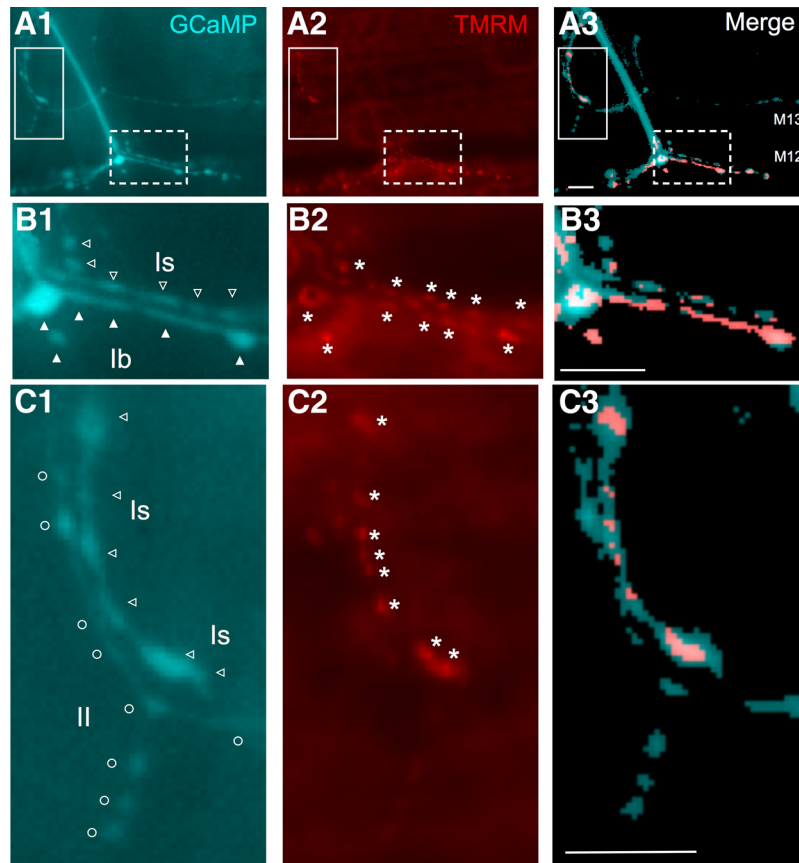


Figure 15. Differential mitochondrial density in type Ib, Is, and II synapses. Columns 1 and 2 are epifluorescent NMJ images obtained with GCaMP1 baseline fluorescence (cyan) and TMRM mitochondrial staining (red), respectively. Column 3 is the merge of columns 1 and 2. The images of the cyan and red channels were separately thresholded before merging to reveal the bouton contour (cyan) and the most strongly stained spots (red). Content in non-bouton, non-axon area was erased in column 3 for clearer demonstration of overlapping. Row **A** is representative images of a muscle 12 (bottom, M12 in **A3**) and 13 (top, M13) NMJs from a WT larva (+/Y; *c164-GCaMP1.3*). The border between M12 and M13 is faintly visible in **A2**. Rows **B**, **C** are enlarged views of the broken and continuous boxed regions in **A**, respectively. In Column 1, type Ib, Is, and II boutons are designated with filled arrowheads, open arrowheads, and open circles, respectively. In Column 2, asterisks indicate some areas of stronger TMRM mitochondrial staining. Note that the weak mitochondrial staining in type II synapses was well below the intensity level of type Is synapses. Statistics are presented in Results.

GCaMP signals (Fig. 16). Action potentials, generated and fine-tuned by Na^+ and K^+ channels, depolarize synaptic terminals and allows Ca^{2+} influx, which triggers synaptic transmission rapidly in milliseconds (Katz and Miledi, 1967; Jan and Jan, 1976; Wu et al., 1978; Zucker, 1996; Südhof and Rothman, 2009). The influx of Ca^{2+} ions are either actively extruded by PMCA locally (Dipolo and Beaugé, 1979), or sequestered by intracellular organelles such as mitochondria (David et al., 1998) and ER (Klose et al., 2009), or buffered by Ca^{2+} binding proteins (Burnashev and Rozov, 2005). The rise of GCaMP signals spans from hundreds of milliseconds up to seconds before peaking, depending on stimulation frequencies and external Ca^{2+} concentrations (Table 2; Figs. 1–3; cf. Reiff et al., 2005; Tian et al., 2009; Akerboom et al., 2012; Chen et al., 2013). Even with improved sensitivity, GCaMP6 signals are not faster compared to GCaMP1.3, taking at least 100 ms after a single stimulus to reach the peak of fluorescence at high external Ca^{2+} concentration (Chen et al., 2013). Thus, GCaMP signals are several orders slower than in-

dividual action potentials and the ensuing postsynaptic potentials (Fig. 9; cf. Xing, 2014; Samigullin et al., 2015). Further, unlike the synthetic Ca^{2+} indicators such as Oregon Green BAPTA (Hill coefficient 1.48; cf. Lnenicka et al., 2006), a GCaMP protein, with calmodulin as the Ca^{2+} sensor, typically binds four Ca^{2+} ions allosterically to produce enhanced fluorescence (Hill coefficients of GCaMP1 = 3.3, GCaMP6m = 2.96; Nakai et al., 2001, Chen et al., 2013). The magnitude of enhancement is thus limited especially at low levels of Ca^{2+} elevations evoked by single action potentials (Rose et al., 2014). Therefore, GCaMP signals better serve as the readout of a leaky integrator that registers cytosolic residual Ca^{2+} , i.e., the net Ca^{2+} accumulation as determined by the process of influx and clearance over repetitive firing of action potentials, which can be induced either by trains of stimulation, or hyperexcitability.

In this study, we used low external Ca^{2+} saline to enhance the differentiation power for detecting presynaptic hyperexcitability. Previous electrophysiological studies

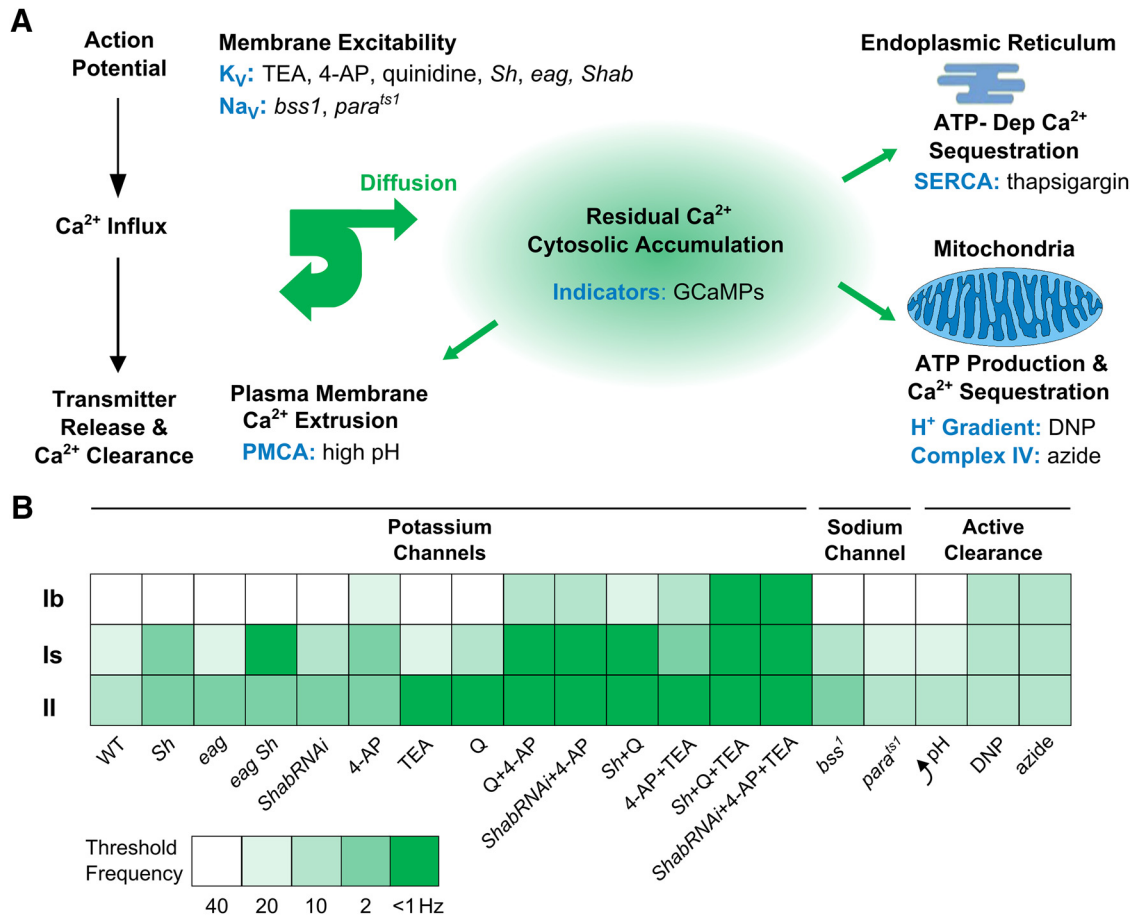


Figure 16. Presynaptic cytosolic residual Ca²⁺ regulation in *Drosophila* NMJ synapses. **A**, Summary diagram of the relevant cellular mechanisms. The targets of manipulations in this study are shown in blue, including Na⁺ and K⁺ channels (Na_v and K_v), PMCA, and H⁺ gradient and Complex IV of mitochondria, together with the corresponding mutational and pharmacological manipulations. **B**, A summary diagram comparing effects of specific experimental manipulations on type Ib, Is, and II synaptic terminals of *c164-GCaMP1.3* and *nSyb-GCaMP6m*. The extent of GCaMP signal enhancement is indicated by reduction in the effective frequencies of stimulation. Threshold frequencies for producing clearly detectable GCaMP signals are color coded. Lower threshold frequencies reflect greater excitability or more hampered Ca²⁺ clearance. More than 1 Hz indicates the cases where individual stimuli evoked the giant hallmark GCaMP signals due to extreme hyperexcitability (compare Figs. 5, 6). 4-AP, 200 μM; TEA, 10 mM; and Q, 20 μM quinidine.

have shown that hyperexcitable mutations such as *bss*, *eag Sh*, and *Sh;;Shab* cause supernumerary high-frequency firing of action potentials in the NMJ nerve bundle at low Ca²⁺ concentrations (Ganetzky and Wu, 1982a, 1983, 1985; Ueda and Wu, 2006). Therefore, we were able to unequivocally delineate among neighboring synaptic terminals the particular synaptic type that displays hyperexcitability based on GCaMP signals. Simultaneous optical and electrophysiological recordings confirmed that only under extreme hyperexcitability conditions, a single stimulus can rise to a giant GCaMP signal due to high-frequency repetitive firing of action potentials over 100 Hz (Figs. 7–9).

Distinct K⁺ and Na⁺ channel control of membrane excitability in tonic type Ib, phasic type Is, and aminergic type II synapses

Electrophysiological recording of postsynaptic EJCs or EJPs generally detects the ensemble effects of type Ib, Is, and II synapses. Unlike type Ib and Is synapses, electro-

physiological characterization of aminergic type II synapses is more technically challenging because they do not generate readily detectable postsynaptic electrical responses. In contrast, GCaMP signals offer the necessary spatial resolution, and thus enabled demonstration for the first time that mutations or blockers of specific ion channels lead to drastically different effects on type II, as well as type Ib and Is, axonal terminals.

As summarized in Figure 16B, our results demonstrated that type Ib synapses were most enriched in the reserve of repolarizing capacity pooled from different K⁺ channel subtypes and could sustain multiple insults of K⁺ channel elimination or blockage before exhibiting the “hallmark” of extreme hyperexcitability (single pulse-evoked giant GCaMP signals at 0.1 mM Ca²⁺; Figs. 5, 6). In comparison, type II synapses had the smallest repertoire of K⁺ channels and simply knocking down either *Shab* or *eag* could induce the hallmark hyperexcitability effect (Fig. 5, right column). In type Is synapses, *Sh* appeared to be the central player for repolarization and perturbing the Sh

Table 4. Statistics table

	Data structure	Type of test	Power
Figure 1B2	Not assumed*	KW tests with Bonferroni correction**	TII vs Tib, $p = 6.60 \times 10^{-15}$ TII vs TIs, $p = 6.31 \times 10^{-18}$
Figure 1B3	Not assumed	KW tests with Bonferroni correction	TII vs TIs, $p = 6.31 \times 10^{-8}$ TIs vs Tib, $p = 3.40 \times 10^{-13}$
Figure 1B4	Not assumed	KW tests with Bonferroni correction	TII vs Tib, $p = 5.90 \times 10^{-13}$ TIs vs Tib, $p = 1.41 \times 10^{-14}$
Figure 2C	Not assumed	KW tests with Bonferroni correction	10 Hz, TII vs Tib, $p = 0.000835$ 10 Hz, TII vs TIs, $p = 3.08 \times 10^{-5}$ 20 Hz, TII vs Tib, $p = 0.000835$ 20 Hz, TIs vs Tib, $p = 0.00706$ 40 Hz, TII vs Tib, $p = 0.000835$ 40 Hz, TIs vs Tib, $p = 0.00706$
Figure 2D	Not assumed	KW tests with Bonferroni correction	2 Hz, TII vs Tib, $p = 0.0628$ 10 Hz, TIs vs Tib, $p = 0.0489$ 10 Hz, TII vs Tib, $p = 0.0271$ 20 Hz, TIs vs Tib, $p = 0.0489$ 40 Hz, TIs vs TII, $p = 0.0628$
Figure 4B	Not assumed	KW tests with Bonferroni correction	TIs, <i>eag Sh</i> vs control, $p = 2.78 \times 10^{-5}$ TIs, 4-AP vs control, $p = 0.0177$ TII, TEA vs control, $p = 0.00942$ TII, <i>eag Sh</i> vs control, $p = 0.0302$
Figure 4D	Not assumed	KW tests with Bonferroni correction	TII, TEA vs control, $p = 0.131$ TIs, 4-AP vs control, $p = 0.0177$ TIs, <i>Sh</i> vs control, $p = 0.00228$ TIs, <i>eag Sh</i> vs control, $p = 4.29 \times 10^{-5}$
Figure 10B	Not assumed	KW tests with Bonferroni correction	TII, 2 Hz, <i>bss1</i> vs control, $p = 0.0337$ TII, 10 Hz, <i>para</i> vs control, $p = 0.0441$ TII, 20 Hz, <i>para</i> vs control, $p = 0.0335$
Figure 13B	Normal	<i>t</i> tests	Tib, 80 Hz, pH 8.8 vs pH 7.2, $p = 0.00665$ TIs, 40 Hz, pH 8.8 vs pH 7.2, $p = 0.00222$ TIs, 80 Hz, pH 8.8 vs pH 7.2, $p = 0.000524$ TII, 10 Hz, pH 8.8 vs pH 7.2, $p = 0.000585$ TII, 20 Hz, pH 8.8 vs pH 7.2, $p = 0.0283$ TII, 40 Hz, pH 8.8 vs pH 7.2, $p = 0.0232$
Figure 13C	Normal	<i>t</i> tests	Tib, 80 Hz, pH 8.8 vs pH 7.2, $p = 0.00665$
Figure 13D	Normal	<i>t</i> tests	TIs, 40 Hz, pH 8.8 vs pH 7.2, $p = 0.0463$
Figure 13E	Normal	ANOVA and Fisher's LSD tests	Tib, 40 Hz, pH 8.8 vs pH 7.2, $p = 0.00665$ TII, 10 Hz, pH 8.8 vs pH 7.2, $p = 0.0358$
Figure 14D	Not assumed	KW tests with Bonferroni correction	Across all boutons and frequencies, Group a vs group b and c, $p < 0.001$ Group b vs group c, $p < 0.05$ Tib, 20 Hz, 60 vs 20 min, $p = 0.013$ Tib, 40 Hz, 60 vs 20 min, $p = 8.78 \times 10^{-9}$ Tib, 40 Hz, 60 min vs NoDNP, $p = 9.11 \times 10^{-9}$ TIs, 10 Hz, 60 vs 20 min, $p = 7.54 \times 10^{-7}$ TIs, 20 Hz, 60 min vs NoDNP, $p = 3.12 \times 10^{-8}$ TIs, 20 Hz, 60 vs 20 min, $p = 0.00206$ TIs, 40 Hz, 60 min vs NoDNP, $p = 2.43 \times 10^{-8}$ TIs, 40 Hz, 60 vs 20 min, $p = 6.14 \times 10^{-8}$ TII, 10 Hz, 20 min vs NoDNP, $p = 0.0126$ TII, 20 Hz, 20 min vs NoDNP, $p = 1.34 \times 10^{-7}$ TII, 40 Hz, 20 min vs NoDNP, $p = 2.61 \times 10^{-10}$
Figure 14E	Not assumed	KW tests with Bonferroni correction	Tib, 40 Hz, 60 min vs NoDNP, $p = 7.24 \times 10^{-5}$ Tib, 40 Hz, 60 vs 20 min, $p = 4.39 \times 10^{-4}$ TIs, 20 Hz, 60 min vs NoDNP, $p = 0.00141$ TIs, 40 Hz, 60 min vs NoDNP, $p = 0.000198$ TII, 20 Hz, 20 min vs NoDNP, $p = 7.23 \times 10^{-7}$ TII, 40 Hz, 20 min vs NoDNP, $p = 7.86 \times 10^{-8}$
Figure 14F	Not assumed	KW tests with Bonferroni correction	Tib, 10 Hz, 60 min vs NoDNP, $p = 2.66 \times 10^{-4}$ Tib, 10 Hz, 60 vs 20 min, $p = 8.05 \times 10^{-5}$ Tib, 20 Hz, 60 vs 20 min, $p = 2.02 \times 10^{-8}$ Tib, 20 Hz, 60 min vs NoDNP, $p = 1.65 \times 10^{-8}$ Tib, 20 Hz, 20 min vs NoDNP, $p = 2.23 \times 10^{-9}$ Tib, 40 Hz, 60 vs 20 min, $p = 8.88 \times 10^{-4}$ Tib, 40 Hz, 60 min vs NoDNP, $p = 9.80 \times 10^{-10}$ Tib, 40 Hz, 20 min vs NoDNP, $p = 1.27 \times 10^{-9}$ TIs, 10 Hz, 60 min vs NoDNP, $p = 4.15 \times 10^{-5}$ TIs, 10 Hz, 20 min vs NoDNP, $p = 8.53 \times 10^{-6}$ TIs, 20 Hz, 60 min vs NoDNP, $p = 0.000114$ TIs, 20 Hz, 20 min vs NoDNP, $p = 0.00312$ TII, 40 Hz, 20 min vs NoDNP, $p = 1.83 \times 10^{-11}$
Figure 15	Normal	<i>t</i> tests with Bonferroni correction	Tib vs TIs, $p = 0.044$ Tib vs TII, $p = 3.73 \times 10^{-13}$ TIs vs TII, $p = 9.46 \times 10^{-6}$

* KW tests do not assume that the data structure is normal.

**All *p* values involving Bonferroni correction have been multiplied with the number of comparisons within the same group of data, whereas the significance levels are set at 0.05, 0.01, and 0.001 for clarity of display in the figures.

channel together with either Eag or Shab channels induced the hallmark ceiling effect of extreme hyperexcitability (Fig. 6). This finding also resolved type Is but not Ib motor axons as the major source of the striking electrophysiological phenotype, i.e., axonal high-frequency repetitive firing (Fig. 9; Ganetzky and Wu, 1982a,b, 1985).

Alleles of *para* also have differential effects on type Ib, Is, and II synapses, possibly reflecting differential expression of the Para product, e.g., different splice isoforms (Thackeray and Ganetzky, 1994; Olson et al., 2008; Lin et al., 2012), or posttranslational modifications.

Type II synapses were more prone to conduction failure on high-frequency stimulation, as indicated by GCaMP signals that frequently became intermittent, or even totally missing during 10- to 40-Hz stimulation (Figs. 10, 11). This reflects the well-known axonal passive cable properties; thinner axons have proportionally higher longitudinal internal resistance relative to trans-membrane resistance, resulting in a more limited safety margin of axonal conduction and a longer refractory period for action potentials (Aidley, 1998). Therefore, type II terminals are more prone to K^+ and Na^+ channels modifications (Figs. 4–6).

Morphometric analysis confirms that the differential excitability and distinct Ca^{2+} dynamics reported here reflect intrinsic properties of type Ib, Is, and II synapses. The GCaMP responses characteristic of each synaptic type were independent of different sizes of boutons along individual axonal synaptic terminals (Fig. 1; cf. Xing and Wu, 2016), implying that differences in the physical dimensions among the three synaptic bouton types do not contribute to the distinct properties of type Ib, Is, and II synapses reported here.

Obviously, besides Na^+ and K^+ channels, other channels may contribute to excitability-controlled Ca^{2+} influx. In particular, different types of Ca^{2+} channels await further study. Notably, previous anatomic studies have shown differences in presynaptic density area among different types of boutons (Atwood et al., 1993; Jia et al., 1993). Ca^{2+} channels are known to be closely associated with active zones embedded within presynaptic density areas. It has been shown that type Is has higher density of active zones than type Ib synapses (He et al., 2009; Lu et al., 2016).

Acute PMCA suppression and long-term inhibition of mitochondrial ATP production: differential effects on different types of synapses

It should be noted that differences in Ca^{2+} clearance capacity correlate well with the distinct frequency responses in the Ca^{2+} dynamics of these synaptic categories. Type II synapses apparently have the slowest rate of Ca^{2+} clearance, as evidenced by its slowest decay of GCaMP signals after secession of stimulation (Figs. 12, 13; Table 3). The faster Ca^{2+} clearance in type Ib than type Is synapses (He et al., 2009) appears to parallel its higher firing frequency (40–60 Hz in Ib vs 10–20 Hz in type Is) during natural bursting activities in semi-intact larval preparations (Cattaert and Birman, 2001; Chouhan et al., 2010), whereas presynaptic cytosolic Ca^{2+} elevation during repetitive firing stimulate mitochondrial oxida-

tive phosphorylation so as to meet temporary burst energy needs (Chouhan et al., 2012). It is conceivable that type Ib synapses thus require a more efficient Ca^{2+} clearance system to avoid intracellular Ca^{2+} build-up. Interestingly, earlier electron microscopy studies have shown that tonic (type Ib) synapses contain more mitochondria than phasic (type Is) synapses in both *Drosophila* larval (Atwood et al., 1993; Jia et al., 1993) and crayfish (Bradacs et al., 1997; Nguyen et al., 1997; Msghina et al., 1998, 1999) NMJs. Our observation using mitochondrial staining confirmed this conclusion and also revealed a far lower density of mitochondria in type II synapses (Fig. 15).

This study showed the importance of mitochondria-powered Ca^{2+} clearance in shaping the distinct dynamics of cytosolic residual Ca^{2+} build-up in type Ib, Is, and II synapses. Inhibiting mitochondrial function with two different means, incubation with either DNP (Fig. 14), a proton ionophore that dissipate mitochondrial proton gradient (Mitchell, 1961; Greenawalt et al., 1964), or azide, an electron-transport chain inhibitor (complex IV), consistently resulted in slower GCaMP signal decay time course and shifted the frequency dependence in type II, Is, and Ib over a period of tens of minutes (Ib, 40–20 Hz; Is, 20–10 Hz).

In contrast to the slow effect of mitochondrial inhibition, high-pH inhibition of PMCA clearly impedes the GCaMP signal decay time course acutely (Figs. 8, 9). Ca^{2+} extrusion via PMCA, a Ca^{2+} -ATPase, has been characterized in the *Drosophila* NMJ (Lnenicka et al., 2006; Niggli and Sigel, 2008), as well as goldfish retina (Zenisek and Matthews, 2000). Although under *in vitro* conditions, the fluorescence intensity of GCaMP protein can be affected by pH change (Nakai et al., 2001), intracellularly expressed GCaMP protein is less likely to be affected by extracellular pH manipulation. This notion was supported by lack of change in presynaptic GCaMP baseline fluorescence intensity on external pH changes ($N = 5$ larvae). Therefore, impaired ATP production from mitochondria can lead to PMCA-mediated Ca^{2+} extrusion shut-down (Fig. 14), which could account for the striking effect of long-term DNP incubation.

Notably, DNP treatment significantly impeded the GCaMP signal decay time course only after long-term incubation (beyond 20 min; Fig. 14). Previous studies employing other proton ionophores such as carbonyl cyanide *m*-chlorophenyl hydrazine (CCCP; Chouhan et al., 2010) has demonstrated that inhibition of mitochondrial proton gradient does not significantly alter overall cytosolic Ca^{2+} dynamics acutely (Lnenicka et al., 2006; Chouhan et al., 2010).

Besides mitochondria, ER may also actively sequester Ca^{2+} via sarco/ER Ca^{2+} ATPase (SERCA) in synapses. We inhibited SERCA with thapsigargin (1–2 μ M, 1-h treatment) and found no obviously detectable effects on GCaMP signals comparable to the effect of DNP on any of the three types of synapses (in 4 larvae). Previous publications with a higher thapsigargin concentration (10 μ M; Klose et al., 2009) or more sensitive Ca^{2+} indicator (Oregon Green BAPTA; Lnenicka et al., 2006) have demonstrated only mildly increased Ca^{2+} signal amplitude and slower time course in type Ib synapses. Therefore, the

contributions of mitochondrial and ER Ca^{2+} sequestration may be masked by other high-capacity ATP-dependent Ca^{2+} clearance mechanisms, such as PMCA. Nevertheless, when ATP production by mitochondria is inhibited, these active Ca^{2+} clearance mechanisms could be diminished on gradual depletion of ATP reserve.

In our study, synapses remain viable, and Ca^{2+} clearance system remains functioning for at least tens of minutes, despite mitochondrial inhibition by DNP or azide (note the unimpaired fast Ca^{2+} clearance at 20 min in Fig. 14). Nonmitochondrial sources of ATP such as glycolysis or ATP binding proteins might sustain for some time, until the first sign of depletion, i.e., the appearance of slower GCaMP signal decay kinetics (Fig. 14).

In fact, some vertebrate central nervous system synapses are known to operate without local presynaptic mitochondria (Budd and Nicholls, 1996; Chavan et al., 2015). Similarly, *Drosophila* mutant *drp1* and *dMiro* larval NMJs, with greatly reduced numbers of synaptic mitochondria, remain viable and display essentially normal Ca^{2+} dynamics and buffer capacity unless challenged by prolonged stimulation beyond minutes (Guo et al., 2005; Verstreken et al., 2005; Chouhan et al., 2010). In our studies, type II synapses had a lower abundance in mitochondria and thus more limited ATP reserve and in consequence were most vulnerable to DNP treatment. They were the first to show lengthened decay and to become completely nonresponsive subsequently during DNP incubation (Fig. 14).

Interpretation of synaptic GCaMP signals

Overall, our study indicates that analysis of GCaMP signals can be extended to extract information about specific synaptic physiologic properties. GCaMP signals offer higher spatial resolution and can complement electrophysiology data to pinpoint critical differences in channel expression and excitability properties among neighboring synaptic terminals.

Systematic kinetic analysis of GCaMP signals revealed the predominant effects of hyperexcitability on the rise kinetics and Ca^{2+} clearance capacity on the decay kinetics. In conjunction with focal electrophysiological recording, genetic and pharmacological analyses indicate a close relationship between GCaMP signals and cytosolic residual Ca^{2+} accumulation rather than the rapid process of Ca^{2+} influx that triggers transmitter release. This approach also revealed the striking hyperexcitable effects caused by insults to multiple K^+ channels, leading to the hallmark giant GCaMP signals evoked by single stimuli that generated high-frequency supernumerary firing of nerve action potentials. Thus, GCaMP signals may be further exploited to shed new light on activity-dependent plasticity in synapses of distinct properties. This work may help to establish guidelines for refined interpretations of GCaMP signals beyond the first-order, qualitative indications for gross neuronal activities in neural circuits.

References

- Aidley DJ (1998) The physiology of excitable cells. Cambridge: Cambridge University Press.
- Akerboom J, Chen TW, Wardill TJ, Tian L, Marvin JS, Mutlu S (2012) Optimization of a GCaMP calcium indicator for neural activity imaging. *J Neurosci* 32:13819–13840. [CrossRef](#) [Medline](#)
- Atwood HL, Govind CK, Wu CF (1993) Differential ultrastructure of synaptic terminals on ventral longitudinal abdominal muscles in *Drosophila* larvae. *J Neurobiol* 24:1008–1024. [CrossRef](#) [Medline](#)
- Benham CD, Evans ML, McBain CJ (1992) Ca^{2+} efflux mechanisms following depolarization evoked calcium transients in cultured rat sensory neurones. *J Physiol* 455:567–583. [Medline](#)
- Berke B, Wittnam J, McNeill E, Van Vactor DL, Keshishian H (2013) Retrograde BMP signaling at the synapse: a permissive signal for synapse maturation and activity-dependent plasticity. *J Neurosci* 33:17937–17950. [CrossRef](#) [Medline](#)
- Bowler MW, Montgomery MG, Leslie AG, Walker JE (2006) How azide inhibits ATP hydrolysis by the F-ATPases. *Proc Natl Acad Sci USA* 103:8646–8649. [CrossRef](#) [Medline](#)
- Bradacs H, Cooper R, Msghina M, Atwood H (1997) Differential physiology and morphology of phasic and tonic motor axons in a crayfish limb extensor muscle. *J Exp Biol* 200:677–691.
- Brüggemann A, Pardo LA, Stühmer W, Pongs O (1993) Ether-à-go-go encodes a voltage-gated channel permeable to K^+ and Ca^{2+} and modulated by cAMP. *Nature* 365:445–448. [CrossRef](#) [Medline](#)
- Buckler KJ, Vaughan-Jones RD (1998) Effects of mitochondrial uncouplers on intracellular calcium, pH and membrane potential in rat carotid body type I cells. *J Physiol* 513:819–833. [CrossRef](#)
- Budd SL, Nicholls DG (1996) A reevaluation of the role of mitochondria in neuronal Ca^{2+} homeostasis. *J Neurochem* 66:403–411. [Medline](#)
- Budnik V, Zhong Y, Wu CF (1990) Morphological plasticity of motor axons in *Drosophila* mutants with altered excitability. *J Neurosci* 10:3754–3768. [Medline](#)
- Burg MG, Wu CF (2012) Mechanical and temperature stressor-induced seizure-and-paralysis behaviors in *Drosophila* bang-sensitive mutants. *J Neurogenet* 26:189–197. [CrossRef](#) [Medline](#)
- Burnashev N, Rozov A (2005) Presynaptic Ca^{2+} dynamics, Ca^{2+} buffers and synaptic efficacy. *Cell Calcium* 37:489–495. [CrossRef](#) [Medline](#)
- Butler A, Wei AG, Baker K, Salkoff L (1989) A family of putative potassium channel genes in *Drosophila*. *Science* 243:943–947. [Medline](#)
- Cattaert D, Birman S (2001) Blockade of the central generator of locomotor rhythm by noncompetitive NMDA receptor antagonists in *Drosophila* larvae. *J Neurobiol* 48:58–73. [Medline](#)
- Caldwell L, Harries P, Sydlik S, Schwiening CJ (2013) Presynaptic pH and vesicle fusion in *Drosophila* larvae neurones. *Synapse* 67:729–740. [CrossRef](#) [Medline](#)
- Chavan V, Willis J, Walker SK, Clark HR, Liu X, Fox MA (2015) Central presynaptic terminals are enriched in ATP but the majority lack mitochondria. *PLoS One* 10:e0125185. [CrossRef](#) [Medline](#)
- Chen L, Koh DS, Hille B (2003) Dynamics of calcium clearance in mouse pancreatic beta-cells. *Diabetes* 52:1723–1731. [Medline](#)
- Chen TW, Wardill TJ, Sun Y, Pulver SR, Renninger SL, Baohan A (2013) Ultrasensitive fluorescent proteins for imaging neuronal activity. *Nature* 499:295–300. [CrossRef](#) [Medline](#)
- Chouhan AK, Zhang J, Zinsmaier KE, Macleod GT (2010) Presynaptic mitochondria in functionally different motor neurons exhibit similar affinities for Ca^{2+} but exert little influence as Ca^{2+} buffers at nerve firing rates *in situ*. *J Neurosci* 30:1869–1881. [CrossRef](#)
- Chouhan AK, Ivannikov MV, Lu Z, Sugimori M, Llinas RR, Macleod GT (2012) Cytosolic calcium coordinates mitochondrial energy metabolism with presynaptic activity. *J Neurosci* 32:1233–1243. [CrossRef](#) [Medline](#)
- David G, Barrett JN, Barrett EF (1998) Evidence that mitochondria buffer physiological Ca^{2+} loads in lizard motor nerve terminals. *J Physiol* 509:59–65. [CrossRef](#)
- Dipolo R, Beaugé L (1979) Physiological role of ATP-driven calcium pump in squid axon. *Nature* 278:271–273. [Medline](#)

- Dipolo R, Beaugé L (1982) The effect of pH on Ca^{2+} extrusion mechanisms in dialyzed squid axons. *Biochim Biophys Acta* 688:237–245. [Medline](#)
- Engel JE, Wu CF (1992) Interactions of membrane excitability mutations affecting potassium and sodium currents in the flight and giant fiber escape systems of *Drosophila*. *J Comp Physiol A Neuroethol Sens Neural Behav Physiol* 171:93–104. [Medline](#)
- Fatt P, Katz B (1952) Spontaneous subthreshold activity at motor nerve endings. *J Physiol* 117:109–128. [Medline](#)
- Fei MJ, Yamashita E, Inoue N, Yao M, Yamaguchi H, Tsukihara T, Shinzawa-Itoh K, Nakashima R, Yoshikawa S (2000) X-ray structure of azide-bound fully oxidized cytochrome c oxidase from bovine heart at 2.9 Å resolution. *Acta Crystallogr D Biol Crystallogr* 56:529–535. [CrossRef](#)
- Feng Y, Ueda A, Wu CF (2004) A modified minimal hemolymph-like solution, HL3.1, for physiological recordings at the neuromuscular junctions of normal and mutant *Drosophila* larvae. *J Neurogenet* 18:377–402. [CrossRef](#) [Medline](#)
- Fox LE, Ueda A, Berke B, Peng IF, Wu CF (2005) Movement disorders in *Drosophila* mutants of potassium channels and biogenic amine pathways. In: *Animal models of movement disorders*, pp 487–504. London: Elsevier Academic Press.
- Fox LE, Soll DR, Wu CF (2006) Coordination and modulation of locomotion pattern generators in *Drosophila* larvae: effects of altered biogenic amine levels by the tyramine beta hydroxylase mutation. *J Neurosci* 26:1486–1498. [CrossRef](#) [Medline](#)
- Frolov RV, Bagati A, Casino B, Singh S (2012) Potassium channels in *Drosophila*: historical breakthroughs, significance, and perspectives. *J Neurogenet* 26:275–290. [CrossRef](#) [Medline](#)
- Ganetzky B, Wu CF (1982a) *Drosophila* mutants with opposing effects on nerve excitability: genetic and spatial interactions in repetitive firing. *J Neurophysiol* 47:501–514.
- Ganetzky B, Wu CF (1982b) Indirect suppression involving behavioral mutants with altered nerve excitability in *Drosophila melanogaster*. *Genetics* 100:597–614.
- Ganetzky B, Wu CF (1983) Neurogenetic analysis of potassium currents in *Drosophila*: synergistic effects on neuromuscular transmission in double mutants. *J Neurogenet* 1:17–28. [Medline](#)
- Ganetzky B, Wu CF (1985) Genes and membrane excitability in *Drosophila*. *Trends Neurosci* 8:322–326. [CrossRef](#)
- Ganetzky B, Wu CF (1986) Neurogenetics of membrane excitability in *Drosophila*. *Annu Rev Genet* 20:13–44. [CrossRef](#) [Medline](#)
- Ganetzky B, Loughney K, Wu CF (1986) Analysis of mutations affecting sodium channels in *Drosophila*. *Ann NY Acad Sci* 479:325–337. [Medline](#)
- Giachello CN, Baines RA (2015) Inappropriate neural activity during a sensitive period in embryogenesis results in persistent seizure-like behavior. *Curr Biol* 25:2964–2968. [CrossRef](#) [Medline](#)
- Greenawalt JW, Rossi CS, Lehninger AL (1964) Effect of active accumulation of calcium and phosphate ions on the structure of rat liver mitochondria. *J Cell Biol* 23:21–38. [Medline](#)
- Guo X, Macleod GT, Wellington A, Hu F, Panchumarthi S, Schoenfeld M (2005) The GTPase dMiro is required for axonal transport of mitochondria to *Drosophila* synapses. *Neuron* 47:379–393. [CrossRef](#) [Medline](#)
- Haugland FN, Wu C-F (1990) A voltage-clamp analysis of gene-dosage effects of the shaker locus on larval muscle potassium currents in *Drosophila*. *J Neurosci* 10:1357–1371.
- He T, Singh V, Rumpal N, Lnenicka GA (2009) Differences in Ca^{2+} regulation for high-output is and low-output is motor terminals in *Drosophila* larvae. *Neuroscience* 159:1283–1291. [CrossRef](#) [Medline](#)
- Higgins ES, Rogers KS (1976) Reversible inhibition of mitochondrial respiratory control by tetrabutylammonium bromide. *Chem Biol Interact* 12:65–69. [Medline](#)
- Hille B (2001) *Ionic channels of excitable membranes*. Sunderland: Sinauer.
- Hoang B, Chiba A (2001) Single-cell analysis of *Drosophila* larval neuromuscular synapses. *Dev Biol* 229:55–70. [CrossRef](#) [Medline](#)
- Hodgkin AL, Keynes RD (1955) Active transport of cations in giant axons from Sepia and Loligo. *J Physiol* 128:28–60. [Medline](#)
- Iverson LE, Tanouye MA, Lester HA, Davidson N, Rudy B (1988) A-type potassium channels expressed from shaker locus cDNA. *Proc Natl Acad Sci USA* 85:5723–5727. [Medline](#)
- Jan LY, Jan YN (1976) L-glutamate as an excitatory transmitter at the *Drosophila* larval neuromuscular junction. *J Physiol* 262:215–236. [Medline](#)
- Jan YN, Jan LY, Dennis MJ (1977) Two mutations of synaptic transmission in *Drosophila*. *Proc R Soc Lond B Biol Sci* 198:87–108. [Medline](#)
- Jia XX, Gorczyca M, Budnik V (1993) Ultrastructure of neuromuscular junctions in *Drosophila*: comparison of wild type and mutants with increased excitability. *J Neurobiol* [Erratum (1994) 25:893–895] 24:1025–1044.
- Johansen J, Halpern ME, Johansen KM, Keshishian H (1989) Stereotypic morphology of glutamatergic synapses on identified muscle cells of *Drosophila* larvae. *J Neurosci* 9:710–725. [Medline](#)
- Kaplan WD, Trout WE 3rd (1969) The behavior of four neurological mutants of *Drosophila*. *Genetics* 61:399–409. [Medline](#)
- Katz B, Miledi R (1967) The timing of calcium action during neuromuscular transmission. *J Physiol* 189:535–544. [Medline](#)
- Katz B, Miledi R (1968) The role of calcium in neuromuscular facilitation. *J Physiol* 195:481–492. [Medline](#)
- Keshishian H, Chiba A, Chang TN, Halfon MS, Harkins EW, Jarecki J (1993) Cellular mechanisms governing synaptic development in *Drosophila melanogaster*. *J Neurobiol* 24:757–787. [CrossRef](#) [Medline](#)
- Klose MK, Boulianne GL, Robertson RM, Atwood HL (2009) Role of ATP-dependent calcium regulation in modulation of *Drosophila* synaptic thermotolerance. *J Neurophysiol* 102:901–913. [CrossRef](#) [Medline](#)
- Koketsu K (1958) Action of tetraethylammonium chloride on neuromuscular transmission in frogs. *Am J Physiol* 193:213–218. [CrossRef](#) [Medline](#)
- Koon AC, Ashley J, Barria R, DasGupta S, Brain R, Waddell S (2011) Autoregulatory and paracrine control of synaptic and behavioral plasticity by octopaminergic signaling. *Nat Neurosci* 14:190–199. [CrossRef](#) [Medline](#)
- Kurdyak P, Atwood HL, Stewart BA, Wu CF (1994) Differential physiology and morphology of motor axons to ventral longitudinal muscles in larval *Drosophila*. *J Comp Neur* 350:463–472. [CrossRef](#) [Medline](#)
- Lee J, Wu CF (2006) Genetic modifications of seizure susceptibility and expression by altered excitability in *Drosophila* Na^+ and K^+ channel mutants. *J Neurophysiol* 96:2465–2478. [CrossRef](#)
- Lee J, Ueda A, Wu CF (2008) Pre- and post-synaptic mechanisms of synaptic strength homeostasis revealed by slowpoke and shaker K^+ channel mutations in *Drosophila*. *Neuroscience* 154:1283–1296. [CrossRef](#)
- Lin WH, Günay C, Marley R, Prinz AA, Baines RA (2012) Activity-dependent alternative splicing increases persistent sodium current and promotes seizure. *J Neurosci* 32:7267–7277. [CrossRef](#) [Medline](#)
- Lnenicka GA, Keshishian H (2000) Identified motor terminals in *Drosophila* larvae show distinct differences in morphology and physiology. *J Neurobiol* 43:186–197. [Medline](#)
- Lnenicka GA, Grizzaffi J, Lee B, Rumpal N (2006) Ca^{2+} dynamics along identified synaptic terminals in *Drosophila* larvae. *J Neurosci* 26:12283–12293. [CrossRef](#) [Medline](#)
- Loughney K, Kreber R, Ganetzky B (1989) Molecular analysis of the *para* locus, a sodium channel gene in *Drosophila*. *Cell* 58:1143–1154. [Medline](#)
- Lu Z, Chouhan AK, Borycz JA, Lu Z, Rossano AJ, Brain KL, Zhou Y, Meinertzhagen IA, Macleod GT (2016) High-probability neurotransmitter release sites represent an energy-efficient design. *Curr Biol* 26:2562–2571. [CrossRef](#)
- MacKinnon R, Yellen G (1990) Mutations affecting TEA blockade and ion permeation in voltage-activated K^+ channels. *Science* 250:276–279. [Medline](#)

- Macleod GT, Hegström-Wojtowicz M, Charlton MP, Atwood HL (2002) Fast calcium signals in *Drosophila* motor neuron terminals. *J Neurophysiol* 88:2659–2663. [CrossRef](#) [Medline](#)
- Macleod GT, Marin L, Charlton MP, Atwood HL (2004) Synaptic vesicles: test for a role in presynaptic calcium regulation. *J Neurosci* 24:2496–2505. [CrossRef](#) [Medline](#)
- Macleod GT, Chen L, Karunanithi S, Peloquin JB, Atwood HL, McRory JE (2006) The *Drosophila* *cac*^{ts2} mutation reduces presynaptic Ca²⁺ entry and defines an important element in Cav2.1 channel inactivation. *Eur J Neurosci* 23:3230–3244. [CrossRef](#) [Medline](#)
- Mao T, O'Connor DH, Scheuss V, Nakai J, Svoboda K (2008) Characterization and subcellular targeting of GCaMP-type genetically encoded calcium indicators. *PLoS One* 3:e1796. [CrossRef](#)
- Melom JE, Littleton JT (2013) Mutation of a NCKX eliminates glial microdomain calcium oscillations and enhances seizure susceptibility. *J Neurosci* 33:1169–1178. [CrossRef](#) [Medline](#)
- Melom JE, Akbergenova Y, Gavornik JP, Littleton JT (2013) Spontaneous and evoked release are independently regulated at individual active zones. *J Neurosci* 33:17253–17263. [CrossRef](#)
- Mitchell P (1961) Coupling of phosphorylation to electron and hydrogen transfer by a chemi-osmotic type of mechanism. *Nature* 191:144–148. [Medline](#)
- Monastriotti M, Gorczyca M, Rapus J, Eckert M, White K, Budnik V (1995) Octopamine immunoreactivity in the fruit fly *Drosophila melanogaster*. *J Comp Neurol* 356:275–287. [CrossRef](#) [Medline](#)
- Mshghina M, Govind CK, Atwood HL (1998) Synaptic structure and transmitter release in crustacean phasic and tonic motor neurons. *J Neurosci* 18:1374–1382. [Medline](#)
- Mshghina M, Millar AG, Charlton MP, Govind CK, Atwood HL (1999) Calcium entry related to active zones and differences in transmitter release at phasic and tonic synapses. *J Neurosci* 19:8419–8434.
- Nakai J, Ohkura M, Imoto K (2001) A high signal-to-noise Ca²⁺ probe composed of a single green fluorescent protein. *Nat Biotechnol* 19:137–141. [CrossRef](#)
- Nguyen PV, Marin L, Atwood HL (1997) Synaptic physiology and mitochondrial function in crayfish tonic and phasic motor neurons. *J Neurophysiol* 78:281–294. [CrossRef](#) [Medline](#)
- Niggli V, Sigel E (2008) Anticipating antiport in P-type ATPases. *Trends Biochem Sci* 33:156–160. [CrossRef](#) [Medline](#)
- Olson RO, Liu Z, Nomura Y, Song W, Dong K (2008) Molecular and functional characterization of voltage-gated sodium channel variants from *Drosophila melanogaster*. *Insect Biochem Mol Biol* 38:604–610. [CrossRef](#) [Medline](#)
- Pak MD, Covarrubias M, Ratcliffe A, Salkoff L (1991) A mouse brain homolog of the *Drosophila* Shab K⁺ channel with conserved delayed-rectifier properties. *J Neurosci* 11:869–880. [Medline](#)
- Parker L, Padilla M, Du Y, Dong K, Tanouye MA (2011) *Drosophila* as a model for epilepsy: *bss* is a gain-of-function mutation in the para sodium channel gene that leads to seizures. *Genetics* 187:523–534. [CrossRef](#) [Medline](#)
- Peng IF, Wu CF (2007) Differential contributions of *Shaker* and *Shab* K⁺ currents to neuronal firing patterns in *Drosophila*. *J Neurophysiol* 97:780–794. [CrossRef](#) [Medline](#)
- Petrenko AY, Cherkashina DV, Somov AY, Tkacheva EN, Semchenko OA, Lebedinsky AS, Fuller BJ (2010) Reversible mitochondrial uncoupling in the cold phase during liver preservation/reperfusion reduces oxidative injury in the rat model. *Cryobiology* 60:293–300. [CrossRef](#) [Medline](#)
- Pongs O, Kecskemethy N, Müller R, Krah-Jentgens I, Baumann A, Kiltz HH, Canal I, Llamazares S, Ferrus A (1988) *Shaker* encodes a family of putative potassium channel proteins in the nervous system of *Drosophila*. *EMBO J* 7:1087–1096. [Medline](#)
- Reiff DF, Ihring A, Guerrero G, Isacoff EY, Joesch M, Nakai J, Borst A (2005) In vivo performance of genetically encoded indicators of neural activity in flies. *J Neurosci* 25:4766–4778.
- Renger JJ, Ueda A, Atwood HL, Govind CK, Wu CF (2000) Role of cAMP cascade in synaptic stability and plasticity: ultrastructural and physiological analyses of individual synaptic boutons in *Drosophila* memory mutants. *J Neurosci* 20:3980–3992. [Medline](#)
- Rickgauer JP, Deisseroth K, Tank DW (2014) Simultaneous cellular-resolution optical perturbation and imaging of place cell firing fields. *Nat Neurosci* 17:1816–1824. [CrossRef](#) [Medline](#)
- Rose T, Goltstein PM, Portugues R, Griesbeck O (2014) Putting a finishing touch on GECIs. *Front Mol Neurosci* 7:88. [CrossRef](#) [Medline](#)
- Sakmann B, Neher E (1984) Patch clamp techniques for studying ionic channels in excitable membranes. *Annu Rev Physiol* 46:455–472. [CrossRef](#) [Medline](#)
- Salkoff LB, Wyman RJ (1983) Ion currents in *Drosophila* flight muscles. *J Physiol* 337:687–709. [Medline](#)
- Samigullin D, Fatikhov N, Khaziev E, Skorinkin A, Nikolsky E, Bukharaeva E (2015) Estimation of presynaptic calcium currents and endogenous calcium buffers at the frog neuromuscular junction with two different calcium fluorescent dyes. *Front Synaptic Neurosci* 6:29. [CrossRef](#)
- Scaduto RC Jr, Grotzohann LW (1999) Measurement of mitochondrial membrane potential using fluorescent rhodamine derivatives. *Biophys J* 76:469–477. [CrossRef](#)
- Schmid A, Chiba A, Doe CQ (1999) Clonal analysis of *Drosophila* embryonic neuroblasts: neural cell types, axon projections and muscle targets. *Development* 126:4653–4689. [Medline](#)
- Schwarz TL, Tempel BL, Papazian DM, Jan YN, Jan LY (1988) Multiple potassium-channel components are produced by alternative splicing at the *Shaker* locus in *Drosophila*. *Nature* [Erratum (1988) 332:740] 331:137–142.
- Shutov LP, Kim MS, Houlihan PR, Medvedeva YV, Usachev YM (2013) Mitochondria and plasma membrane Ca²⁺-ATPase control presynaptic Ca²⁺ clearance in capsaicin-sensitive rat sensory neurons. *J Physiol* 591:2443–2462. [CrossRef](#)
- Siddiqi O, Benzer S (1976) Neurophysiological defects in temperature-sensitive *paralytic* mutants of *Drosophila melanogaster*. *Proc Natl Acad Sci USA* 73:3253–3257. [Medline](#)
- Singh A, Singh S (1999) Unmasking of a novel potassium current in *Drosophila* by a mutation and drugs. *J Neurosci* 19:6838–6843. [Medline](#)
- Singh S, Wu CF (1989) Complete separation of four potassium currents in *Drosophila*. *Neuron* 2:1325–1329. [Medline](#)
- Stewart BA, Atwood HL, Renger JJ, Wang J, Wu CF (1994) Improved stability of *Drosophila* larval neuromuscular preparations in haemolymph-like physiological solutions. *J Comp Physiol A Neuroethol Sens Neural Behav Physiol* 175:179–191. [Medline](#)
- Südhof TC, Rothman JE (2009) Membrane fusion: grappling with SNARE and SM proteins. *Science* 323:474–477. [CrossRef](#) [Medline](#)
- Suzuki DT, Grigliatti T, Williamson R (1971) Temperature-sensitive mutations in *Drosophila melanogaster*. VII. A mutation (*para-ts*) causing reversible adult paralysis. *Proc Natl Acad Sci USA* 68:890–893. [Medline](#)
- Suzuki N, Wu CF (1984) Altered sensitivity to sodium channel-specific neurotoxins in cultured neurons from temperature-sensitive *paralytic* mutants of *Drosophila*. *J Neurogenet* 1:225–238. [Medline](#)
- Suzuki S, Osanai M, Mitsumoto N, Akita T, Narita K, Kijima H (2002) Ca²⁺-dependent Ca²⁺ clearance via mitochondrial uptake and plasmalemmal extrusion in frog motor nerve terminals. *J Neurophysiol* 87:1816–1823. [CrossRef](#)
- Tang Y, Zucker RS (1997) Mitochondrial involvement in post-tetanic potentiation of synaptic transmission. *Neuron* 18:483–491. [Medline](#)
- Thackeray JR, Ganetzky B (1994) Developmentally regulated alternative splicing generates a complex array of *Drosophila* para sodium channel isoforms. *J Neurosci* 14:2569–2578.
- Thesleff S (1980) Aminopyridines and synaptic transmission. *Neuroscience* 5:1413–1419. [Medline](#)
- Tian L, Hires SA, Mao T, Huber D, Chiappe ME, Chalasani SH (2009) Imaging neural activity in worms, flies and mice with improved GCaMP calcium indicators. *Nat Methods* 6:875–881. [CrossRef](#) [Medline](#)

- Timpe LC, Schwarz TL, Tempel BL, Papazian DM, Jan YN, Jan LY (1988a) Expression of functional potassium channels from *Shaker* cDNA in *Xenopus* oocytes. *Nature* 331:143–145.
- Timpe LC, Jan YN, Jan LY (1988b) Four cDNA clones from the *Shaker* locus of *Drosophila* induce kinetically distinct A-type potassium currents in *Xenopus* oocytes. *Neuron* 1:659–667.
- Torroja L, Packard M, Gorczyca M, White K, Budnik V (1999) The *Drosophila* beta-amyloid precursor protein homolog promotes synapse differentiation at the neuromuscular junction. *J Neurosci* 19:7793–7803.
- Tsunoda S, Salkoff L (1995) The major delayed rectifier in both *Drosophila* neurons and muscle is encoded by *Shab*. *J Neurosci* 15:5209–5221.
- Ueda A, Wu CF (2006) Distinct frequency-dependent regulation of nerve terminal excitability and synaptic transmission by IA and IK potassium channels revealed by *Drosophila* *shaker* and *shab* mutations. *J Neurosci* 26:6238–6248. [CrossRef Medline](#)
- Ueda A, Wu CF (2009a) Role of rut adenylyl cyclase in the ensemble regulation of presynaptic terminal excitability: reduced synaptic strength and precision in a *Drosophila* memory mutant. *J Neurogenet* 23:185–199.
- Ueda A, Wu CF (2009b) Effects of social isolation on neuromuscular excitability and aggressive behaviors in *Drosophila*: altered responses by *Hk* and *gsts1*, two mutations implicated in redox regulation. *J Neurogenet* 23:378–394.
- Ueda A, Wu CF (2012) Cyclic adenosine monophosphate metabolism in synaptic growth, strength, and precision: neural and behavioral phenotype-specific counterbalancing effects between *dnc* phosphodiesterase and *rut* adenylyl cyclase mutations. *J Neurogenet* 26:64–81. [CrossRef Medline](#)
- Ueda A, Wu CF (2015) The role of cAMP in synaptic homeostasis in response to environmental temperature challenges and hyperexcitability mutations. *Front Cell Neurosci* 9:10. [CrossRef](#)
- Verstreken P, Ly CV, Venken KJ, Koh TW, Zhou Y, Bellen HJ (2005) Synaptic mitochondria are critical for mobilization of reserve pool vesicles at *Drosophila* neuromuscular junctions. *Neuron* 47:365–378. [CrossRef Medline](#)
- Walker JA, Gouzi JY, Long JB, Huang S, Maher RC, Xia H (2013) Genetic and functional studies implicate synaptic overgrowth and ring gland cAMP/PKA signaling defects in the *Drosophila* melanogaster neurofibromatosis-1 growth deficiency. *PLoS Genet* 9:e1003958. [CrossRef Medline](#)
- Wang JW, Wong AM, Flores J, Vossell LB, Axel R (2003) Two-photon calcium imaging reveals an odor-evoked map of activity in the fly brain. *Cell* 112:271–282. [Medline](#)
- Wang Y, Guo HF, Pologruto TA, Hannan F, Hakker I, Svoboda K (2004) Stereotyped odor-evoked activity in the mushroom body of *Drosophila* revealed by green fluorescent protein-based Ca^{2+} imaging. *J Neurosci* 24:6507–6514. [CrossRef Medline](#)
- Warmke J, Drysdale R, Ganetzky B (1991) A distinct potassium channel polypeptide encoded by the *Drosophila* *eag* locus. *Science* 252:1560–1562. [Medline](#)
- Wong MY, Zhou C, Shakiryanova D, Lloyd TE, Deitcher DL, Levitan ES (2012) Neuropeptide delivery to synapses by long-range vesicle circulation and sporadic capture. *Cell* 148:1029–1038. [Cross-Ref Medline](#)
- Wu CF, Ganetzky B (1980) Genetic alteration of nerve membrane excitability in temperature-sensitive *paralytic* mutants of *Drosophila melanogaster*. *Nature* 286:814–816. [Medline](#)
- Wu CF, Ganetzky B, Haugland FN, Liu AX (1983) Potassium currents in *Drosophila*: different components affected by mutations of two genes. *Science* 220:1076–1078. [Medline](#)
- Wu CF, Haugland FN (1985) Voltage clamp analysis of membrane currents in larval muscle fibers of *Drosophila*: alteration of potassium currents in *shaker* mutants. *J Neurosci* 5:2626–2640. [Medline](#)
- Wu CF, Ganetzky B, Jan LY, Jan YN, Benzer S (1978) A *Drosophila* mutant with a temperature-sensitive block in nerve conduction. *Proc Natl Acad Sci USA* 75:4047–4051. [Medline](#)
- Wu CF, Tsai MC, Chen ML, Zhong Y, Singh S, Lee CY (1989) Actions of dendrotoxin on K^+ channels and neuromuscular transmission in *Drosophila melanogaster*, and its effects in synergy with K^+ channel-specific drugs and mutations. *J Exp Biol* 147:21–41.
- Xing X (2014) Genetic and functional analysis of synaptic Ca^{2+} dynamics in *Drosophila*. The University of Iowa.
- Xing X, Wu CF (2016) Distinct Ca^{2+} dynamics in glutamatergic and aminergic synapses determined by intrinsic neuronal properties independent of synaptic bouton physical dimensions and GCaMP expression levels. *Soc Neurosci Poster* 400.15/F42.
- Zenisek D, Matthews G (2000) The role of mitochondria in presynaptic calcium handling at a ribbon synapse. *Neuron* 25:229–237. [Medline](#)
- Zhang D, Kuromi H, Kidokoro Y (1999) Activation of metabotropic glutamate receptors enhances synaptic transmission at the *Drosophila* neuromuscular junction. *Neuropharmacology* 38:645–657. [Medline](#)
- Zhong Y, Wu CF (2004) Neuronal activity and adenylyl cyclase in environment-dependent plasticity of axonal outgrowth in *Drosophila*. *J Neurosci* 24:1439–1445. [CrossRef Medline](#)
- Zhong Y, Budnik V, Wu CF (1992) Synaptic plasticity in *Drosophila* memory and hyperexcitable mutants: role of cAMP cascade. *J Neurosci* 12:644–651. [Medline](#)
- Zucker RS (1996) Exocytosis: a molecular and physiological perspective. *Neuron* 17:1049–1055. [Medline](#)
- Zucker RS, Regehr WG (2002) Short-term synaptic plasticity. *Annu Rev Physiol* 64:355–405. [CrossRef Medline](#)